ELSEVIER

Chemical Geology 207 (2004) 237–259

CHEMICAL GEOLOGY
INCLUDING
ISOTOPE GEOSCIENCE

www.elsevier.com/locate/chemgeo

Evidence for subduction-related components in the subcontinental mantle from low $^{3}He/^{4}He$ and $^{40}Ar/^{36}Ar$ ratio in mantle xenoliths from Far Eastern Russia

Junji Yamamoto[a,b,*], Ichiro Kaneoka[c,1], Shun'ichi Nakai[c,2], Hiroyuki Kagi[d,3], Vladimir S. Prikhod'ko[e,4], Shoji Arai[f,5]

[a] *Institute for Geothermal Sciences, Kyoto University, Noguchibaru, Beppu, Ooita-pref. 874-0903, Japan*
[b] *Centre de Recherches Pétrographiques et Géochimiques, 15 rue Notre Dame des Pauvres 54501 Vandoeuvre les Nancy, France*
[c] *Earthquake Research Institute, University of Tokyo, 1-1-1 Yayoi, Bunkyo, Tokyo 113-0032, Japan*
[d] *Laboratory for Earthquake Chemistry, University of Tokyo, 7-3-1 Hongo, Bunkyo, Tokyo 113-0033, Japan*
[e] *Institute of Tectonics and Geophysics (Far-Eastern Branch, Russian Academy of Sciences), 65 Kim Yu Chen Street, Khabarovsk 680063, Russia*
[f] *Department of Earth Sciences, Faculty of Science, Kanazawa University, Kakuma, Kanazawa 920-1192, Japan*

Received 26 June 2003; accepted 14 March 2004

Abstract

By applying both vacuum crushing and stepwise heating methods for the extraction of the noble gases, we have discovered $^{3}He/^{4}He$ ratios much lower than the atmospheric ratio ($\sim 0.3\ R_A$; R_A is the atmospheric $^{3}He/^{4}He$ ratio of 1.4×10^{-6}) and relatively low $^{40}Ar/^{36}Ar$ ratios (<1000) in olivine separates from some subcontinental mantle-derived xenoliths from Far Eastern Russia. The low $^{3}He/^{4}He$ ratios cannot be explained by the addition of radiogenic ^{4}He generated in-situ after the eruption of magma entraining the xenoliths. Furthermore, petrographic evidence suggests that incorporation of crustal fluids is not likely. Hence, it must reflect a feature of the Far Eastern Russian upper mantle.

Spectroscopic and petrographic observations confirm that there are at least two compositionally distinct fluids in these xenoliths; liquid CO_2 inclusions and melt inclusions with shrinkage bubbles. Based on the crushing experiments, it is inferred that the inclusions of liquid CO_2 have a $^{3}He/^{4}He$ ratio similar to that of MORB, and the component with the low $^{3}He/^{4}He$ ratio is derived from the shrinkage bubbles in the melt inclusions.

For the present samples, the $^{40}Ar/^{36}Ar$ ratios obtained by crushing were less than 1000, suggesting incorporation of atmospheric components in the source materials. Since low $^{40}Ar/^{36}Ar$ ratios were observed irrespective of the occurrence of the liquid CO_2 inclusions, the atmospheric component exists in the melt inclusions. Ne and Xe isotopes are also consistent with incorporation of atmospheric components.

* Corresponding author. Institute for Geothermal Sciences, Kyoto University, Noguchibaru, Beppu, Ooita-pref. 874-0903, Japan. Tel.: +81-977-22-0713; fax: +81-977-22-0965.

E-mail addresses: jyama@bep.vgs.kyoto-u.ac.jp (J. Yamamoto), kaneoka@eri.u-tokyo.ac.jp (I. Kaneoka), snakai@eri.u-tokyo.ac.jp (S. Nakai), kagi@eqchem.s.u-tokyo.ac.jp (H. Kagi), vladimir@itig.as.khb.ru (V.S. Prikhod'ko), ultrasa@kenroku.ipc.kanazawa-u.ac.jp (S. Arai).

[1] Tel.: +81-3-5841-5770; fax: +81-3-5802-3391.
[2] Tel.: +81-3-5841-5698; fax: +81-3-5802-3391.
[3] Tel.: +81-3-5841-7625; fax: +81-3-5841-8366.
[4] Tel.: +7-1-509-689-3295x3080; fax: +7-4212-22-76-84.
[5] Tel.: +81-76-264-5726; fax: +81-76-264-5746.

doi:10.1016/j.chemgeo.2004.03.007

Since the Far Eastern Russia area was located at a subduction zone in the Jurassic–early Cretaceous Period, it is most likely that the melt inclusions displaying atmospheric noble gas characteristics together with low $^3He/^4He$ ratios have been derived from the Jurassic–Cretaceous subducted slab. Although we cannot exclude the possibility that low $^3He/^4He$ ratios are due to the existence of minor U-bearing minerals in the lithospheric continental mantle caused by metasomatism, we have no petrographical evidence for such minerals in this area. On the other hand, $^3He/^4He$ ratios observed in the liquid CO_2 inclusions, which are similar to the MORB-like value, might reflect the general character of the upper mantle. The Far Eastern Russian mantle may therefore be a MORB-like source that has been partly infiltrated by subduction-related fluids.

Keywords: Noble gases; Mantle xenolith; Lherzolite; Fluid inclusion; Subduction; Far Eastern Russia

1. Introduction

The source of mid-ocean ridge basalts (MORB) is generally regarded to be the suboceanic upper mantle (e.g., Kaneoka, 1983). The $^3He/^4He$ ratios of MORB show quite uniform values of around 8 R_A (Craig and Lupton, 1976; Rison, 1980; Kurz and Jenkins, 1981). On the other hand, low $^3He/^4He$ ratios compared to those of MORBs are reported from some subcontinental ultramafic xenoliths (Kyser and Rison, 1982; Nagao and Takahashi, 1993; Dunai and Baur, 1995; Matsumoto et al., 1997; Dodson and Brandon, 1999). In most previous studies of subcontinental lithospheric mantle materials, gases were extracted by the heating method, in which extracted gases include trapped, radiogenic and/or nucleogenic components generated within the crystal lattice after eruption of magma entraining the xenoliths. It should be emphasized that all the data reported so far by other workers which indicate $^3He/^4He$ ratios lower than the atmospheric value are limited to heating samples such as apatite (Matsumoto et al., 1997), clinopyroxene (Dunai and Baur, 1995) and whole rock (Kyser and Rison, 1982), which are considered to contain larger amount of U and Th than olivine. Olivine is relatively retentive for helium (Kurz, 1986; Trull et al., 1991), and in-situ addition of radiogenic ^4He generated from U and Th is considered to be quite small due to their very low contents in olivine (e.g., Porcelli et al., 1986). Further, the crushing method is thought to be effective in extracting noble gases trapped in liquid inclusions or shrinkage bubbles in melt inclusions, which contain little in-situ generated nuclides (e.g. Kurz et al., 1983; Kurz, 1986; Porcelli et al., 1987; Graham et al., 1992a,b; Patterson et al., 1997; Scarsi, 2000). Gautheron and Moreira (2002) suggest a value of 6.1 ± 0.9 R_A for helium in the subcontinental lithospheric mantle using published data where helium was obtained only by crushing of olivines from phenocrysts or xenoliths. However, careful selection of olivines only from spinel peridotite, which is a typical rock of the upper-most mantle, shows a mean $^3He/^4He$ ratio comparable to that of MORB (Matsumoto et al., 1998; Matsumoto et al., 2000). It is noted that relatively low $^3He/^4He$ ratios (4.2 R_A) have been reported for olivine separates from mantle wedge-derived spinel peridotites by crushing (Dodson and Brandon, 1999).

The aim of this paper is to determine the noble gas characteristics in the subcontinental lithospheric mantle and obtain constraints on the influences of subducted components. For this purpose, a combination of crushing and stepwise-heating methods were applied in order to extract noble gases from mantle wedge-derived materials and identify specific mantle components in the mantle wedge. To get information on the contribution of the subduction-related components, mantle-derived xenoliths from the subduction zone are suitable. In particular, in regions where old slabs have been stored in the mantle, the noble gas compositions of the mantle may be different from those in present arcs due to accumulation of the radiogenic nuclides with time. We therefore analyzed all noble gas isotopes in olivine separates from mantle-derived ultramafic xenoliths from Far Eastern Russia. We also measured the U concentration in olivine to evaluate the influence of radiogenic nuclides. In addition, microspectroscopy and petrographic observation were used to provide independent information on their spatial distribution of the subduction-related components.

2. Samples

In Far Eastern Russia, extensive basaltic volcanism occurred in the Cenozoic Period, and the alkaline

volcanic rocks contain abundant upper mantle-derived ultramafic xenoliths (Fig. 1). Far Eastern Russia was an active margin of the Eurasian continent in the Mesozoic to Paleogene Period (Burrett, 1974; Maruyama and Sakai, 1986; Faure and Natal'in, 1992). In this area, subcontinental lithospheric mantle would be affected by subduction-related fluids.

The xenoliths sampled comprise mainly spinel-lherzolites, with rare harzburgites and dunites. The xenoliths were taken from different volcanic bodies of seven regions with eruption ages from about 0.3–14 Ma (Okamura et al., 1998; Sato, 1999; Tatsumi et al., 2000; Rasskazov et al., 2000; Fig. 1). Xenoliths are up to about 10 cm long. They have protogranular textures and consist of olivine, orthopyroxene, and clinopyroxene with lesser amounts of spinel. The average size of these minerals is about 0.5 mm in diameter. All xenoliths used in this study show major element compositions typical of upper mantle rocks. For example, the Fo values [100 × Mg/(Mg + Fe) of olivine] and the Cr# [Cr/(Cr + Al)] of spinel show uniform values ranging from 88 to 91 and from 0.09 to 0.12, respectively (Yamamoto, 2001). They are located within the Olivine Spinel Mantle Array (OSMA; proposed by Arai, 1987). The textures and zoning profiles of the constituent minerals suggest that the xenoliths have experienced a simple history of cooling and heating before reaching the surface. The heating episode due to entrainment by the host magma is represented by reaction coronae surrounding the xenoliths, but it is limited to the rim of the marginal minerals. Further, the equilibrium temperatures estimated by the two-pyroxene geothermometer range from 800 to 1100 °C (Yamamoto, 2001), less than the temperature of alkaline basaltic eruptions (approximately 1200 °C) (Ionov et al., 1995). Consequently, mineral equilibria in the xenoliths were not disturbed by incorporation of the xenoliths into the host magma.

Gases extracted by crushing minerals are released mostly from fluid inclusions (Moore, 1979; Kurz et al., 1983; Scarsi, 2000). We defined the fluid inclusion having liquid or gas state and solid one as liquid inclusion and melt one, respectively. At least two compositionally distinct groups of fluid inclusions are observed in the minerals (Fig. 2). Liquid inclusions have negative crystal shape and are dominantly composed of CO_2 (Yamamoto et al., 2002). In addition to CO_2, Raman microscopic analyses reveal graphite on the interface between host minerals and liquid CO_2 inclusions. CH_4, H_2O, N_2 and CO were not detected. The liquid CO_2 inclusions are rarely >20 μm in size, and are usually <10 μm. The second group of inclusions are elongated and vermicular melt inclusions. The melt inclusions are often accompanied with a hydrous mineral, which is detected using micro-Raman spectroscopic analysis (Yamamoto, 2001). The liquid CO_2

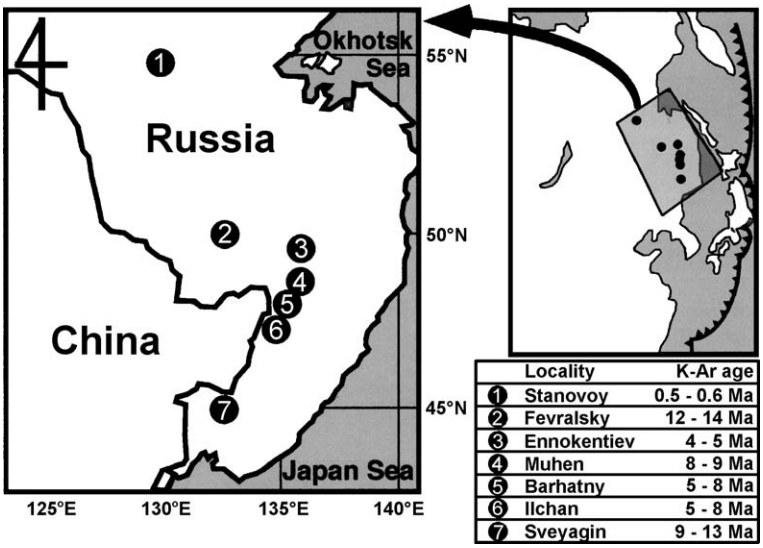

Fig. 1. Sample localities and K–Ar ages of the volcanic bodies (Sato, 1999; Okamura et al., 1998; Tatsumi et al., 2000; Rasskazov et al., 2000).

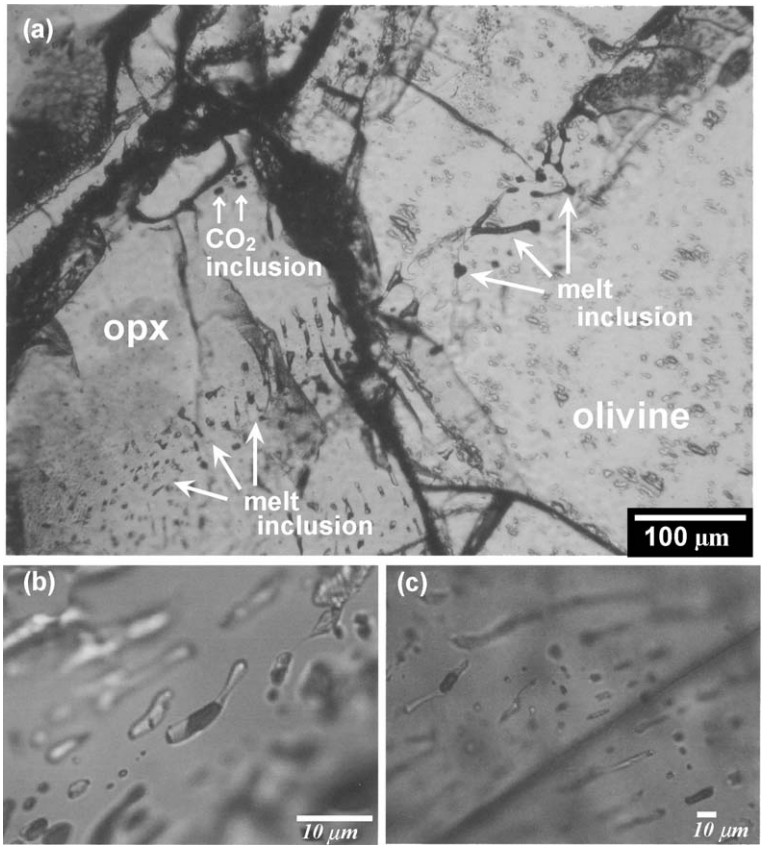

Fig. 2. Photomicrographs of a xenolith thin section from Far Eastern Russia. (a) A photograph around the grain boundary between olivine and orthopyroxene. Two generations of inclusions are visible. The first is decorated by vermicular melt inclusions within a plane of the section. The melt inclusion crosscut the grain boundary. The second is indicated by fluid inclusion arrays. (b) A photo shows a number of vermicular melt inclusions in an olivine of Sv-1. An inclusion located almost at the center contains a vapor bubble. (c) Similar inclusions as seen in photo (b) are also observed in En2I.

inclusions are aligned, traverse the entire length of the crystal, but do not crosscut grain boundaries, and are not uniformly distributed among the localities. For example, the xenoliths from Sveyagin and Fevralsky do not contain liquid CO_2 inclusions. Melt inclusions along healed fractures are observed in all the Far Eastern Russian mantle-derived xenoliths studied. They are frequently traced across grain boundaries (Fig. 2a). The size of melt inclusions is in the same range as those of liquid CO_2 inclusions.

In some cases, liquid CO_2 inclusions are penetrated by melt inclusions, and these liquid CO_2 inclusions often contain vapor bubbles. This may indicate that the liquid CO_2 inclusions were formed initially as a liquid phase. Bubbles are also observed in melt inclusions, which have been formed by shrinkage of the melt during cooling, and would be a host for noble gases extracted by crushing. Detailed descriptions of each sample and relations between host magma, inclusions of liquid CO_2 and melt are shown in Appendices A and B, respectively.

3. Experimental method

3.1. Noble gas analyses

Minerals were carefully separated by handpicking, removing altered parts and impurities. Grains were soaked in 2 N HNO_3 for half an hour at 70 °C, then washed ultrasonically in distilled water, ethanol and acetone. To extract gases by crushing, samples were

loaded into a crusher mill and baked at 150–200 °C overnight. Before crushing, crushing vessels were preheated at 120 °C for more than an hour. During crushing, the crushed sample together with the vessel was heated at 120 °C. Gases extracted were exposed to a cold trap at liquid nitrogen temperature in order to remove gases adsorbed on newly created powder surfaces. The crushing yield, defined as the fraction of the crushed material ($\leq$150 μm), range from 12% to 90%.

Based on preliminary stepwise degassing experiments (Tables 5 and 6) using temperature intervals of one or two hundred degrees from 600 to 1900 °C for an aliquot of the same olivine as used here, we adopted four temperature steps (600, 1000, 1600 and 1900 °C). Preliminary experiments suggest that degassing of inclusion-hosted gases occurs at 1000 °C, but adsorbed atmospheric gases are mostly degassed at 600 °C. Cosmogenic ^{3}He is mostly degassed at 1600 °C and the remaining component degassed at 1900 °C due to melting of olivine. Duration of heating is 40, 30, 25 and 20 min for the fractions of 600, 1000, 1600 and 1900 °C, respectively.

Helium and neon were separated from argon, krypton and xenon using a cold trap with activated charcoal at liquid nitrogen temperature. Helium and neon were further separated at around − 215 °C using a cryogenic refrigerator with activated charcoal prior to analysis. Most of the argon was separated from krypton and xenon prior to analysis using a cold trap with activated charcoal cooled to − 65 °C by mixture of ethanol and dry ice. Separation of krypton and xenon were not performed due to the difficulty of separation using cold trap.

Noble gas analyses were performed on a sector-type mass spectrometer VG-5400 installed at the Earthquake Research Institute, University of Tokyo, which is equipped with three collectors; a Faraday cup (FC), a Daly photomultiplier and an electron multiplier (EM)-based ion counting system.

The procedural crushing blanks for ^{4}He and ^{3}He were typically less than 2.0×10^{-11} and 3.0×10^{-15} cm^3 STP, respectively. The procedural heating blanks for ^{4}He and ^{3}He at each temperature step were less than 2.0×10^{-10} and 9.0×10^{-15} cm^3 STP, respectively. Linearity of the helium isotope ratio with the ^{3}He content was guaranteed down to the range of 1×10^{-15} cm^3 STP (after blank correction) by repeated analyses of the diluted air standard and two types of standard gases (artificial helium standard gas (20.63 ± 0.10 R_A; Sumino et al., 2001; Matsuda et al., 2002) and Kaminoyama well gas, Yamagata, Japan (6.04 ± 0.29 R_A; Hanyu et al., 1999). Typical errors for ^{4}He and ^{3}He abundances (>1×10^{-14} cm^3 STP/g) are less than 35% and 15%, respectively. The uncertainties in the precision (1σ) include those for the sensitivity and blank corrections. Procedural crushing blanks for ^{20}Ne, ^{36}Ar, ^{84}Kr and ^{132}Xe were less than 2×10^{-12}, 1×10^{-12}, 2×10^{-14} and 4×10^{-15} cm^3 STP, respectively. Procedural heating blanks for ^{20}Ne, ^{36}Ar, ^{84}Kr and ^{132}Xe at each temperature step were less than 6×10^{-12}, 1×10^{-11}, 5×10^{-13} and 1×10^{-13} cm^3 STP, respectively. The uncertainty for all noble gas abundances except for helium is about 5% at 1σ. More detailed analytical conditions for noble gases at the ERI have been reported by Hanyu et al. (1999).

3.2. U analyses

Uranium analyses were undertaken on olivine separates from some mantle-derived xenoliths. Olivine separates were washed with 2 N HNO_3 for half an hour at 70 °C and washed ultrasonically in distilled water. After the treatment, about 100 mg of olivine of each sample was weighed in a Teflon beaker, finely crushed in an agate mortar then dried. About 20 mg of powder was dissolved in 7 N $HClO_4$ and 30 N HF in capped beakers, agitated in an ultrasonic bath for 30 min and heated while sealed at 160 °C for 12 h. A total of 0.5 ml of 200 ppb indium and rhenium nitrate solutions were added as internal standards. The solution was analyzed with an inductively coupled plasma-mass spectrometry (ICP-MS) (PQ3, Thermoelemental, UK) at Earthquake Research Institute, University of Tokyo. Procedural blanks were less than 20 pg. The uncertainty for abundance of uranium is less than 10% (except for Fev-1 where only a maximum possible value is listed in Table 3 due to a U content lower than the detection limit).

4. Results

4.1. Isotope composition of noble gases

4.1.1. Helium

Noble gas isotope results are summarized in Tables 1–6. For gases extracted by crushing, ^{3}He/^{4}He ratios

Table 1
Noble gas abundances (crushing results)

Sample	Mineral	Weight (g)	^{3}He (10^{-14})	^{4}He (10^{-9})	^{20}Ne (10^{-12})	^{21}Ne (10^{-14})	^{22}Ne (10^{-13})	^{36}Ar (10^{-12})	^{40}Ar (10^{-9})	^{84}Kr (10^{-12})	^{132}Xe (10^{-14})
Ennokentiev											
En-1	olivine	1.539	3.77 ± 0.55	3.446 ± 0.010	47.6 ± 1.2	*	*	107.11 ± 0.25	43.30 ± 0.13	3.562 ± 0.038	32.0 ± 1.3
En-44	olivine	1.442	0.99 ± 0.24	1.25 ± 0.12	9.6 ± 1.0	2.92 ± 0.49	9.71 ± 1.06	30.2 ± 1.8	16.45 ± 0.98	0.828 ± 0.084	4.38 ± 0.40
En-010	olivine	0.877	0.51 ± 0.44	0.98 ± 0.13	166 ± 21	49.9 ± 6.7	168 ± 21	320 ± 19	103.1 ± 6.1	8.45 ± 0.52	28.4 ± 1.9
En-41	olivine	0.893	0.38 ± 0.38	0.76 ± 0.10	8.8 ± 1.1	2.60 ± 0.47	9.0 ± 1.2	22.0 ± 1.3	10.08 ± 0.60	0.652 ± 0.050	5.00 ± 0.47
En2A	olivine	1.221	1.31 ± 0.45	1.61 ± 0.21	18.1 ± 2.3	5.51 ± 0.89	17.7 ± 2.3	31.7 ± 1.9	12.42 ± 0.74	1.162 ± 0.084	10.95 ± 0.72
En2I	olivine	1.871	< 0.1	0.241 ± 0.031	3.42 ± 0.43	0.96 ± 0.29	3.70 ± 0.58	4.66 ± 0.28	2.04 ± 0.12	0.193 ± 0.018	2.87 ± 0.21
En2I	opx	1.603	< 0.1	0.436 ± 0.057	9.3 ± 1.2	2.76 ± 0.62	9.8 ± 1.4	4.77 ± 0.29	5.91 ± 0.35	0.199 ± 0.015	3.71 ± 0.27
En2I	cpx	1.063	0.13 ± 0.13	1.02 ± 0.14	162 ± 20	47.8 ± 6.4	162 ± 20	38.7 ± 2.3	19.7 ± 1.2	1.229 ± 0.080	11.46 ± 0.83
Ilchanska											
Ilc-1	olivine	1.433	0.42 ± 0.34	0.735 ± 0.002	19.89 ± 0.55	5.57 ± 0.66	18.5 ± 1.1	27.460 ± 0.089	11.503 ± 0.039	1.635 ± 0.026	54.9 ± 1.5
Ilc-2	olivine	1.131	0.42 ± 0.28	0.099 ± 0.017	0.91 ± 0.10	b.l.	1.07 ± 0.43	6.21 ± 0.40	3.96 ± 0.24	0.544 ± 0.048	2.44 ± 0.28
Ilc-2	olivine	0.920	b.l.	0.287 ± 0.037	30.2 ± 3.8	8.71 ± 1.43	30.7 ± 3.9	51.8 ± 3.1	16.23 ± 0.97	1.298 ± 0.085	5.69 ± 0.50
Sveyagin											
Sv-1	olivine	1.187	0.15 ± 0.32	3.708 ± 0.023	4.96 ± 0.18	1.58 ± 0.32	5.16 ± 0.39	18.378 ± 0.029	7.575 ± 0.015	0.521 ± 0.012	4.52 ± 0.26
Sv2-10	olivine	1.212	< 0.1	0.309 ± 0.032	5.54 ± 0.60	1.71 ± 0.82	4.5 ± 1.2	21.7 ± 1.3	8.68 ± 0.51	2.24 ± 0.13	47.9 ± 2.9
Sv3-02	olivine	1.745	b.l	b.l.	3.50 ± 0.36	1.3 ± 2.1	3.78 ± 0.50	17.0 ± 1.0	5.19 ± 0.31	0.601 ± 0.045	4.22 ± 0.33
Sv-2	olivine	0.752	b.l.	0.299 ± 0.039	31.6 ± 4.0	9.5 ± 1.4	31.8 ± 4.1	73.7 ± 4.4	22.8 ± 1.4	2.29 ± 0.15	11.61 ± 0.93
Sv2J	olivine	1.535	0.24 ± 0.27	1.46 ± 0.19	7.9 ± 1.0	2.23 ± 0.57	7.8 ± 1.2	16.56 ± 0.99	5.27 ± 0.31	0.663 ± 0.044	12.19 ± 0.82
Sv2G	olivine	1.542	b.l.	0.413 ± 0.054	2.33 ± 0.31	0.64 ± 0.31	2.11 ± 0.49	7.95 ± 0.47	2.56 ± 0.15	0.400 ± 0.027	7.39 ± 0.50
Sv2H	olivine	1.611	b.l.	0.90 ± 0.12	2.99 ± 0.40	0.76 ± 0.32	2.72 ± 0.54	8.39 ± 0.50	3.96 ± 0.24	0.412 ± 0.029	6.81 ± 0.47
Sv2F	olivine	1.717	< 0.1	1.87 ± 0.25	12.8 ± 1.6	3.72 ± 0.63	13.0 ± 1.7	22.8 ± 1.4	7.57 ± 0.45	1.063 ± 0.065	18.6 ± 1.2
Sv2F	opx	1.116	< 0.1	1.01 ± 0.13	3.82 ± 0.50	1.09 ± 0.50	4.25 ± 0.80	5.64 ± 0.34	2.67 ± 0.16	0.211 ± 0.024	5.26 ± 0.37
Sv2F	cpx	1.809	< 0.1	1.09 ± 0.15	17.9 ± 2.2	5.53 ± 0.88	18.1 ± 2.3	11.77 ± 0.70	11.66 ± 0.70	0.458 ± 0.033	10.33 ± 0.69
Fevralsky											
Fev-1	olivine	0.790	0.22 ± 0.33	12.918 ± 0.047	5.91 ± 0.39	2.79 ± 0.75	8.89 ± 0.96	16.605 ± 0.061	7.174 ± 0.026	0.388 ± 0.015	2.38 ± 0.17
Fev#-4	olivine	1.762	0.38 ± 0.25	0.464 ± 0.042	3.67 ± 0.61	2.2 ± 7.9	4.6 ± 1.7	8.24 ± 0.50	5.87 ± 0.35	0.264 ± 0.026	2.55 ± 0.20
Fev-16	olivine	0.795	b.l.	0.301 ± 0.048	24.0 ± 3.9	7.0 ± 2.0	25.3 ± 5.5	50.2 ± 3.0	15.19 ± 0.91	1.26 ± 0.10	5.78 ± 0.51
Barhatny											
Ba-1	olivine	1.498	0.30 ± 0.38	0.275 ± 0.002	27.75 ± 0.82	7.78 ± 0.74	26.7 ± 1.6	57.995 ± 0.071	16.962 ± 0.023	1.350 ± 0.014	7.06 ± 0.37
Ba-2	olivine	1.360	0.15 ± 0.64	0.012 ± 0.015	10.7 ± 1.1	4.98 ± 0.79	11.2 ± 1.3	15.72 ± 0.95	4.83 ± 0.29	0.415 ± 0.056	091 ± 0.23
Ba-17	olivine	1.075	b.l.	0.035 ± 0.045	6.6 ± 1.2	b.l.	6.7 ± 1.4	12.71 ± 0.99	4.74 ± 0.37	0.270 ± 0.050	1.83 ± 0.30
Ba-18	olivine	0.814	b.l.	0.107 ± 0.022	12.5 ± 1.6	4.08 ± 0.62	13.5 ± 1.8	38.3 ± 2.3	11.35 ± 0.68	1.086 ± 0.074	5.94 ± 0.52
Muhen											
Mu-2	olivine	0.866	b.l.	11.227 ± 0.045	27.67 ± 0.75	8.26 ± 0.75	28.6 ± 1.8	71.74 ± 0.17	22.892 ± 0.063	1.562 ± 0.030	6.67 ± 0.30
Stanovoy											
St-5	olivine	1.458	b.l.	0.444 ± 0.070	24.0 ± 3.0	6.8 ± 1.1	23.4 ± 3.0	47.9 ± 2.9	14.43 ± 0.86	1.437 ± 0.096	22.6 ± 1.5

N.B., unit for abundance is cm^3 STP/g. All tabulated data were corrected for blanks. b.l.: blank level, meaning abundance of measured gas is smaller than blank. *: not measured.

Table 2
Noble gas isotopic ratios (crushing results)

Sample	Mineral	Weight (g)	$^{3}He/^{4}He$ (R/R_A)	$^{20}Ne/^{22}Ne$	$^{21}Ne/^{22}Ne$	$^{40}Ar/^{36}Ar$	$^{38}Ar/^{36}Ar$	$^{4}He/^{40}Ar^{*}$
Ennokentiev								
En-1	olivine	1.539	7.8 ± 1.2	*	*	407.4 ± 7.7	0.1865 ± 0.0010	0.2875 ± 0.0055
En-44	olivine	1.442	6.5 ± 1.8	9.92 ± 0.35	0.0301 ± 0.0039	544.9 ± 6.1	0.1885 ± 0.0024	0.166 ± 0.019
En-010	olivine	0.877	3.2 ± 2.8	9.89 ± 0.16	0.0297 ± 0.0013	321.9 ± 3.3	0.1899 ± 0.0012	0.116 ± 0.017
En-41	olivine	0.893	3.1 ± 3.1	9.72 ± 0.34	0.0288 ± 0.0035	457.9 ± 5.5	0.1889 ± 0.0021	0.214 ± 0.031
En2A	olivine	1.221	4.9 ± 1.6	10.18 ± 0.33	0.0311 ± 0.0029	392.0 ± 3.7	0.1890 ± 0.0011	0.527 ± 0.076
En2I	olivine	1.871	0.8 ± 2.5	9.26 ± 0.86	0.0260 ± 0.0068	438.1 ± 4.3	0.1869 ± 0.0017	0.363 ± 0.052
En2I	opx	1.603	0.1 ± 1.9	9.44 ± 0.55	0.0282 ± 0.0050	1239 ± 12	0.1876 ± 0.0022	0.097 ± 0.014
En2I	cpx	1.063	0.77 ± 0.77	10.00 ± 0.16	0.0295 ± 0.0012	508.9 ± 4.6	0.1880 ± 0.0010	0.124 ± 0.018
Ilchanska								
Ilc-1	olivine	1.433	4.0 ± 3.7	10.76 ± 0.58	0.0301 ± 0.0031	423.9 ± 8.0	0.1880 ± 0.0011	0.2086 ± 0.0041
Ilc-2	olivine	1.131	27 ± 22	8.50 ± 3.24	*	638 ± 23	0.1891 ± 0.0097	0.0466 ± 0.0089
Ilc-2	olivine	0.920	< 7.1	9.82 ± 0.23	0.0284 ± 0.0029	313.2 ± 3.3	0.1892 ± 0.0016	0.312 ± 0.045
Sveyagin								
Sv-1	olivine	1.187	0.28 ± 0.68	9.60 ± 0.64	0.0307 ± 0.0057	397.7 ± 4.0	0.1888 ± 0.0011	1.974 ± 0.024
Sv2-10	olivine	1.212	0.6 ± 2.8	12.21 ± 2.90	0.0376 ± 0.0153	400.6 ± 4.0	0.1887 ± 0.0024	0.136 ± 0.016
SV3-02	olivine	1.745	< 504	9.24 ± 0.76	0.0333 ± 0.0559	304.9 ± 3.0	0.1889 ± 0.0023	*
Sv-2	olivine	0.752	< 7.3	9.93 ± 0.30	0.0298 ± 0.0022	309.9 ± 3.3	0.1891 ± 0.0014	0.281 ± 0.040
Sv2J	olivine	1.535	1.0 ± 1.1	10.12 ± 0.84	0.0285 ± 0.0058	318.5 ± 2.9	0.1873 ± 0.0014	3.83 ± 0.55
Sv2G	olivine	1.542	< 0.78	11.04 ± 2.12	0.0301 ± 0.0127	321.9 ± 2.9	0.1888 ± 0.0011	1.97 ± 0.28
Sv2H	olivine	1.611	< 0.50	10.99 ± 1.63	0.0278 ± 0.0102	472.2 ± 4.3	0.1888 ± 0.0012	0.607 ± 0.087
Sv2F	olivine	1.717	0.01 ± 0.24	9.90 ± 0.31	0.0287 ± 0.0032	331.5 ± 3.0	0.1876 ± 0.0008	2.27 ± 0.33
Sv2F	opx	1.116	0.3 ± 1.5	9.00 ± 1.22	0.0257 ± 0.0108	473.0 ± 4.6	0.1884 ± 0.0023	1.01 ± 0.14
Sv2F	cpx	1.809	0.22 ± 0.69	9.87 ± 0.26	0.0305 ± 0.0028	990.8 ± 9.6	0.1878 ± 0.0013	0.134 ± 0.020
Fevralsky								
Fev-1	olivine	0.790	0.12 ± 0.22	*	0.0314 ± 0.0077	418.2 ± 4.3	0.1873 ± 0.0011	6.342 ± 0.073
Fev#-4	olivine	1.762	4.6 ± 3.6	8.02 ± 2.64	0.0488 ± 0.1717	712 ± 13	0.1873 ± 0.0044	0.135 ± 0.015
Fev-16	olivine	0.795	< 13.7	9.48 ± 1.38	0.0276 ± 0.0050	302.5 ± 3.4	01895 ± 0.0021	0.86 ± 0.15
Barhatny								
Ba-1	olivine	1.498	8 ± 11	10.41 ± 0.56	0.0292 ± 0.0021	294.5 ± 5.6	0.1877 ± 0.0010	*
Ba-2	olivine	1.360	79 ± 351	9.57 ± 0.40	0.0445 ± 0.0050	307.1 ± 4.3	0.1895 ± 0.0034	0.067 ± 0.085
Ba-17	olivine	1.075	< 204	9.94 ± 0.88	*	372.5 ± 8.5	0.1864 ± 0.0058	0.035 ± 0.046
Ba-18	olivine	0.814	< 20.8	9.29 ± 0.39	0.0303 ± 0.0022	295.9 ± 3.6	0.1894 ± 0.0019	6.7 ± 1.4
Muhen								
Mu-2	olivine	0.866	< 0.23	9.69 ± 0.53	0.0289 ± 0.0019	307.1 ± 3.1	0.18794 ± 0.00083	13.50 ± 0.15
Stavonoy								
St-5	olivine	1.458	< 1.5	10.26 ± 0.32	0.0291 ± 0.0030	301.3 ± 2.7	0.18726 ± 0.00057	1.60 ± 0.27

N.B., All tabulated data were corrected for blanks. $^{40}AR^{*}$ is ^{40}AR corrected for air-addition. *: not measured.

vary greatly from ~ 8 R_A (En-1) down to < 1 R_A (Fev. and Sv. samples) (Table 2). Values of ~ 0.3 R_A are found for Fev-1, Sv2F and Sv-1. Although the ^{3}He blanks correspond to almost 50% of the observed ^{3}He signals for Fev-1, Sv2F and Sv-1, even if the ^{3}He blanks varied by 50%, the $^{3}He/^{4}He$ ratios for these samples would not exceed 1 R_A due to their high ^{4}He contents. Although the ^{3}He content of Mu-2 could not be distinguished from the blank, its $^{3}He/^{4}He$ ratio must be less than 0.28 R_A. Olivine, opx and cpx of En2I and

Table 3
Noble gas
(heating results) and uranium contents in olivines of spinel lherzolites

Sample	Weight (g)	Temperature (°C)	^{3}He (10^{-14})	^{4}He (10^{-9})	^{20}Ne (10^{-12})	^{21}Ne (10^{-12})	^{22}Ne (10^{-12})	^{36}Ar (10^{-12})	^{40}Ar (10^{-9})	^{84}Kr (10^{-12})	^{132}Xe (10^{-14})	^{238}U (pbb)
En-1	0.914	600	0.19 ± 0.46	0.403 ± 0.056	9.3 ± 1.8	0.024 ± 0.018	1.06 ± 0.26	21.2 ± 1.6	6.38 ± 0.48	0.748 ± 0.059	6.36 ± 0.71	
		1000	3.98 ± 0.66	2.69 ± 0.35	24.9 ± 4.6	0.075 ± 0.015	2.48 ± 0.46	81.6 ± 6.2	25.1 ± 1.9	2.61 ± 0.22	17.2 ± 1.5	
		1600	7.6 ± 1.1	3.55 ± 0.46	14.3 ± 2.6	0.084 ± 0.026	1.55 ± 0.33	45.1 ± 3.4	42.0 ± 3.2	1.58 ± 0.15	11.8 ± 1.5	
		1900	4.48 ± 0.82	4.39 ± 0.57	21.8 ± 4.0	0.087 ± 0.019	2.13 ± 0.40	89.1 ± 6.7	72.4 ± 5.5	3.26 ± 0.26	30.9 ± 2.7	
		total	16.3 ± 1.6	11.03 ± 0.82	70.3 ± 6.9	0.269 ± 0.058	7.20 ± 0.82	237.0 ± 9.9	145.8 ± 6.6	8.20 ± 0.38	66.2 ± 3.5	8.41 ± 0.79
llc-1	0.718	600	0.11 ± 0.37	0.449 ± 0.064	0.49 ± 0.17	0.0015 ± 0.0058	0.057 ± 0.054	59.1 ± 4.5	17.9 ± 1.3	3.65 ± 0.28	71.3 ± 6.1	
		1000	2.36±0.51	3.77±0.49	3.66±0.69	0.0116±0.0070	0.40±0.11	41.6±3.1	13.8±1.0	3.34±0.25	34.4±3.0	
		1600	10.8 ± 1.6	2.31 ± 0.30	28.7 ± 5.3	0.093 ± 0.018	2.77 ± 0.51	14.3 ± 1.1	14.7 ± 1.1	1.78 ± 0.14	26.9 ± 2.5	
		1900	1.45 ± 0.54	1.03 ± 0.14	69 ± 13	0.249 ± 0.048	6.8 ± 1.3	23.3 ± 1.8	38.7 ± 2.9	0.474 ± 0.074	2.73 ± 0.75	
		total	14.8 ± 1.8	7.56 ± 0.60	102 ± 14	0.355 ± 0.057	10.0 ± 1.4	138.4 ± 5.8	85.2 ± 3.6	9.25 ± 0.41	135.2 ± 7.3	26.3 ± 2.5
Sv-1	07.59	600	1.64 ± 0.42	41.9 ± 5.5	47.3 ± 8.7	0.147 ± 0.30	4.84 ± 0.90	143 ± 11	44.0 ± 3.3	5.21 ± 0.39	40.2 ± 3.1	
		1000	12.1 ± 1.7	260 ± 34	16.1 ± 3.0	0.079 ± 0.019	2.51 ± 0.48	50.2 ± 3.8	15.0 ± 1.1	1.69 ± 0.14	13.6 ± 1.3	
		1600	11.5 ± 1.7	57.9 ± 7.5	21.2 ± 3.9	0.117 ± 0.028	2.39 ± 0.46	54.4 ± 4.1	20.8 ± 1.6	1.74 ± 0.13	14.2 ± 1.3	
		1900	1.00 ± 0.44	0.86 ± 0.12	46.4 ± 8.5	0.197 ± 0.039	4.63 ± 0.86	183 ± 14	67.4 ± 5.1	5.56 ± 0.44	37.7 ± 3.0	
		total	26.3 ± 2.5	360 ± 35	131 ± 13	0.534 ± 0.077	14.1 ± 1.5	431 ± 18	147.1 ± 6.4	14.20 ± 0.62	105.7 ± 4.7	16.9 ± 1.3
Fev-1	0.589	600	0.32 ± 0.61	4.49 ± 0.59	1.03 ± 0.24	0.005 ± 0.014	0.021 ± 0.035	7.43 ± 0.62	2.25 ± 0.19	0.514 ± 0.052	10.8 ± 1.1	
		1000	4.6 ± 1.2	71.9 ± 9.4	2.56 ± 0.57	0.020 ± 0.035	0.19 ± 0.17	10.44 ± 0.84	3.63 ± 0.30	0.597 ± 0.059	9.0 ± 1.1	
		1600	3.48 ± 0.99	8.0 ± 1.0	3.24 ± 0.86	0.024 ± 0.022	0.37 ± 0.18	6.35 ± 0.56	2.91 ± 0.24	0.363 ± 0.045	4.9 ± 1.2	
		1900	0.62 ± 0.61	0.362 ± 0.066	7.1 ± 2.2	0.043 ± 0.080	1.11 ± 0.86	7.65 ± 0.91	5.05 ± 0.38	0.362 ± 0.037	0.44 ± 0.20	
		total	9.0 ± 1.8	84.8 ± 9.4	13.9 ± 2.4	0.09 ± 0.16	1.2 ± 1.2	31.9 ± 1.5	13.85 ± 0.57	1.84 ± 0.10	25.2 ± 2.0	< 4.6
Ba-1	0.956	600	1.28 ± 0.38	68.1 ± 8.9	1.99 ± 0.39	0.0078 ± 0.0061	0.312 ± 0.090	5.78 ± 0.44	2.42 ± 0.18	0.357 ± 0.035	9.19 ± 0.81	
		1000	4.03 ± 0.62	4.95 ± 0.65	1.88 ± 0.37	0.0102 ± 0.0091	0.200 ± 0.090	9.82 ± 0.74	3.33 ± 0.25	0.464 ± 0.048	8.96 ± 0.87	
		1600	7.4 ± 1.2	0.248 ± 0.041	1.77 ± 0.37	0.025 ± 0.017	0.177 ± 0.083	6.01 ± 0.46	2.87 ± 0.22	0.237 ± 0.023	4.79 ± 0.52	
		1900	0.16 ± 0.42	0.011 ± 0.017	2.99 ± 0.58	0.047 ± 0.020	0.37 ± 0.10	5.77 ± 0.44	2.46 ± 0.19	0.138 ± 0.013	1.21 ± 0.57	
		total	12.9 ± 1.5	73.3 ± 8.9	8.63 ± 0.87	0.093 ± 0.052	1.03 ± 0.33	27.4 ± 1.1	11.09 ± 0.43	1.197 ± 0.065	24.2 ± 1.4	
Mu-2	0.597	600	0.51 ± 0.45	0.448 ± 0.067	1.04 ± 0.43	0.003 ± 0.019	0.21 ± 0.23	6.87 ± 0.56	2.05 ± 0.17	0.31 ± 0.11	2.01 ± 0.27	
		1000	13.4 ± 1.8	6.55 ± 0.85	1.55 ± 0.46	0.015 ± 0.017	0.18 ± 0.13	11.93 ± 0.97	3.67 ± 0.30	0.617 ± 0.048	8.65 ± 0.87	
		1600	12.3 ± 2.3	0.453 ± 0.079	2.41 ± 0.53	0.073 ± 0.038	0.39 ± 0.15	11.7 ± 1.1	3.87 ± 0.37	0.597 ± 0.061	11.7 ± 1.6	
		1900	b.l.	0.033 ± 0.041	2.27 ± 0.53	0.045 ± 0.025	0.26 ± 0.10	9.46 ± 0.72	3.66 ± 0.28	0.366 ± 0.045	2.2 ± 1.0	
		total	26.1 ± 3.1	7.48 ± 0.86	7.26 ± 0.98	0.134 ± 0.097	0.99 ± 0.48	39.9 ± 1.8	13.26 ± 0.58	1.89 ± 0.14	24.6 ± 2.1	

N.B., unit for abundance is cm^3 STP/g, except for U. All tabulated data were corrected for blanks. b.l.: blank level, which is case when abundance of measured gas is lower than that of blank.

Table 4
Noble gas isotopic ratio (heating results)

Sample	Weight (g)	Temperature (°C)	$^{3}He/^{4}He$ (R/R_A)	$^{20}Ne/^{22}Ne$	$^{21}Ne/^{22}Ne$	$^{40}Ar/^{36}Ar$	$^{38}Ar/^{36}Ar$	$^{4}He/^{40}Ar^{*}$
En-1	0.914	600	3.1 ± 7.4	8.8 ± 1.3	0.022 ± 0.016	300.4 ± 2.7	0.1878 ± 0.0021	3.85 ± 0.61
		1000	9.6 ± 1.2	10.03 ± 0.20	0.0301 ± 0.0027	307.1 ± 2.1	0.1887 ± 0.0010	2.84 ± 0.43
		1600	14.0 ± 1.4	9.25 ± 0.97	0.054 ± 0.012	929.4 ± 7.1	0.1894 ± 0.0016	0.124 ± 0.019
		1900	6.67 ± 0.95	10.19 ± 0.38	0.0410 ± 0.0042	812.5 ± 5.5	0.1891 ± 0.0011	0.095 ± 0.014
		total	9.66 ± 0.83	9.76 ± 0.56	0.0373 ± 0.0069	620.0 ± 4.0	0.18890 ± 0.00091	0.143 ± 0.012
Ilc-1	0.718	600	1.6 ± 5.3	8.6 ± 7.5	0.026 ± 0.098	302.4 ± 2.1	0.1888 ± 0.0013	1.11 ± 0.18
		1000	4.08 ± 0.74	9.1 ± 1.7	0.029 ± 0.016	332.4 ± 2.3	0.1888 ± 0.0014	2.46 ± 0.37
		1600	30.7 ± 2.6	10.37 ± 0.24	0.0336 ± 0.0019	1031 ± 11	0.1871 ± 0.0040	0.220 ± 0.033
		1900	9.0 ± 3.3	10.17 ± 0.28	0.0364 ± 0.0019	1661 ± 12	0.1879 ± 0.0025	0.032 ± 0.005
		total	13.3 ± 1.2	10.18 ± 0.35	0.0353 ± 0.0029	623.7 ± 4.1	0.1885 ± 0.0011	0.167 ± 0.015
Sv-1	0.759	600	0.26 ± 0.06	9.78 ± 0.27	0.0305 ± 0.0024	306.9 ± 2.1	0.1887 ± 0.0010	25.7 ± 3.9
		1000	0.31 ± 0.02	6.41 ± 0.30	0.0315 ± 0.0049	298.7 ± 2.1	0.1898 ± 0.0011	1606 ± 242
		1600	1.29 ± 0.12	8.90 ± 0.53	0.0492 ± 0.0069	382.0 ± 2.7	0.1890 ± 0.0015	12.3 ± 1.9
		1900	7.4 ± 3.2	10.01 ± 0.31	0.0426 ± 0.0030	368.5 ± 2.6	0.1901 ± 0.0011	0.064 ± 0.010
		total	0.478 ± 0.036	9.31 ± 0.33	0.0379 ± 0.0036	340.7 ± 2.2	0.18942 ± 0.00087	18.5 ± 2.0
Fev-1	0.589	600	0.47 ± 0.88	48 ± 76	0.23 ± 0.51	304 ± 16	0.190 ± 0.012	75 ± 12
		1000	0.42 ± 0.10	13 ± 11	0.11 ± 0.16	348 ± 11	0.1920 ± 0.0071	131 ± 20
		1600	2.83 ± 0.74	8.8 ± 3.7	0.067 ± 0.051	459 ± 22	0.187 ± 0.011	7.7 ± 1.3
		1900	11 ± 12	6.4 ± 4.6	0.039 ± 0.066	659 ± 34	0.197 ± 0.017	0.130 ± 0.029
		total	0.69 ± 0.13	11 ± 11	0.07 ± 0.11	429.3 ± 9.5	0.1919 ± 0.0059	19.9 ± 2.4
Ba-1	0.956	600	0.123 ± 0.034	6.4 ± 1.3	0.025 ± 0.018	420 ± 10	0.1885 ± 0.0049	95 ± 14
		1000	5.32 ± 0.55	9.4 ± 3.8	0.051 ± 0.039	339.5 ± 3.4	0.1892 ± 0.0027	11.5 ± 1.7
		1600	193 ± 90	10.0 ± 4.2	0.140 ± 0.070	477.4 ± 6.4	0.1838 ± 0.0050	0.227 ± 0.042
		1900	88 ± 269	8.1 ± 1.6	0.127 ± 0.041	427.1 ± 5.5	0.1893 ± 0.0054	0.015 ± 0.022
		total	1.012 ± 0.093	8.4 ± 2.6	0.090 ± 0.041	404.4 ± 3.7	0.1879 ± 0.0022	24.6 ± 3.1
Mu-2	0.579	600	7.4 ± 7.2	5.0 ± 5.1	0.015 ± 0.089	299 ± 15	0.189 ± 0.011	21.7 ± 3.8
		1000	13.42 ± 0.93	8.7 ± 5.6	0.084 ± 0.078	308 ± 15	0.189 ± 0.011	44.7 ± 7.2
		1600	175 ± 84	6.1 ± 1.9	0.185 ± 0.068	331.8 ± 5.3	0.1873 ± 0.0039	1.07 ± 0.22
		1900	< 121	8.8 ± 2.8	0.174 ± 0.066	387.3 ± 7.7	0.1891 ± 0.0074	0.038 ± 0.048
		total	20.9 ± 1.9	7.3 ± 3.4	0.136 ± 0.072	330.8 ± 6.2	0.1886 ± 0.0044	5.31 ± 0.66

N.B., all tabulated were corrected for blanks. $^{40}Ar^{*}$ is ^{40}Ar corrected for air-addition.

Sv2F samples show similar $^{3}He/^{4}He$ ratios (and similar ^{4}He concentrations within a factor of 2–5) (Fig. 3). This may indicate that these minerals have trapped the same fluid (see Appendix B) and that post-eruptive processes have not significantly affected $^{3}He/^{4}He$ ratio. By contrast, one sample (En-1) shows a $^{3}He/^{4}He$ ratio (7.8 ± 1.2 R_A) as observed in MORB. En-44 and En2A from the same region as En-1 also show relatively high $^{3}He/^{4}He$ ratios (6.5 ± 1.8 and 4.9 ± 1.6 R_A, respectively). Overall, the xenoliths from Ennokentiev (En-series) display relatively high $^{3}He/^{4}He$ ratios (3.1–7.8 R_A) or show a positive correlation between He content and isotopic ratio. The $^{3}He/^{4}He$ ratios therefore vary among different localities. The En2I sample is from the same region as En-1 but shows low $^{3}He/^{4}He$ ratios (0.1–0.8 R_A). The same is observed in the samples from Sveyagin (Sv-series) (0.01–1.0 R_A). These results suggest the existence of at least two kinds of fluids within the Far Eastern Russian mantle-derived xenoliths.

For gases extracted by heating, the $^{3}He/^{4}He$ ratios obtained in the 1000 °C fractions correspond roughly to those of crush-released helium (Tables 2 and 4). Cosmogenic ^{3}He might affect some of the 1600 °C fractions as seen in the high $^{3}He/^{4}He$ ratios particularly for Mu-2 and Ba-1. Although the amounts of gases extracted by crushing are less than the total amounts of gases extracted by heating, a rough agreement is observed between the $^{3}He/^{4}He$ ratios by total heating and those by crushing. This indicates that the gases extracted by crushing almost represent the total $^{3}He/^{4}He$ ratios especially for the samples with low $^{3}He/^{4}He$ ratios. Furthermore, the He should be located in a phase that can be extracted by the

Table 5
Noble gas abundance of a spinel lherzolite (stepwise heating results)

Sample	Mineral	Weight (g)	Temperature (°C)	^{3}He (10^{-14})	^{4}He (10^{-9})	^{20}Ne (10^{-12})	^{36}Ar (10^{-12})	^{40}Ar (10^{-9})	^{84}Kr (10^{-12})	^{132}Xe (10^{-14})
En2I	olivine	1.512	600	0.21 ± 0.18	1.97 ± 0.29	3.86 ± 0.48	2.42 ± 0.15	0.805 ± 0.048	0.284 ± 0.017	10.87 ± 0.71
			700	0.81 ± 0.28	3.08 ± 0.42	2.60 ± 0.32	2.75 ± 0.17	0.989 ± 0.059	0.1122 ± 0.0066	4.41 ± 0.29
			800	1.07 ± 0.31	2.05 ± 0.27	2.26 ± 0.28	11.96 ± 0.72	3.61 ± 0.22	0.1227 ± 0.0073	3.64 ± 0.24
			1000	3.00 ± 0.51	1.63 ± 0.23	1.96 ± 0.25	3.10 ± 0.19	1.204 ± 0.072	0.0997 ± 0.0059	3.85 ± 0.25
			1200	6.5 ± 1.1	0.96 ± 0.13	2.72 ± 0.34	3.86 ± 0.23	2.07 ± 0.12	0.1521 ± 0.0090	6.75 ± 0.44
			1400	4.34 ± 0.73	0.336 ± 0.053	5.87 ± 0.73	7.47 ± 0.45	3.34 ± 0.20	0.327 ± 0.019	8.95 ± 0.58
			1600	2.46 ± 0.41	0.258 ± 0.035	3.67 ± 0.46	3.79 ± 0.23	2.26 ± 0.14	0.180 ± 0.011	3.87 ± 0.25
			1900	1.00 ± 0.30	0.376 ± 0.072	8.4 ± 1.0	7.19 ± 0.43	5.75 ± 0.34	0.346 ± 0.020	7.76 ± 0.51
			total	19.4 ± 1.5	10.67 ± 0.64	31.3 ± 1.6	42.5 ± 1.0	20.03 ± 0.50	1.623 ± 0.038	50.1 ± 1.3
En2I	opx	1.575	600	1.50 ± 0.30	5.75 ± 0.75	12.7 ± 1.6	2.22 ± 0.13	0.939 ± 0.056	0.237 ± 0.014	10.59 ± 0.69
			700	1.75 ± 0.50	2.97 ± 0.39	9.6 ± 1.2	13.94 ± 0.83	4.73 ± 0.28	0.189 ± 0.011	6.59 ± 0.43
			800	1.71 ± 0.46	1.68 ± 0.23	5.25 ± 0.66	1.147 ± 0.070	1.419 ± 0.085	0.0396 ± 0.0023	2.27 ± 0.15
			1000	6.6 ± 1.3	3.23 ± 0.45	5.98 ± 0.75	2.79 ± 0.17	2.67 ± 0.16	0.1283 ± 0.0076	5.57 ± 0.36
			1200	5.45 ± 0.85	1.98 ± 0.26	8.0 ± 1.0	2.70 ± 0.16	6.06 ± 0.36	0.1443 ± 0.0086	11.48 ± 0.75
			1400	1.13 ± 0.28	0.571 ± 0.085	8.2 ± 1.0	2.39 ± 0.15	8.94 ± 0.53	0.0796 ± 0.0047	4.06 ± 0.27
			1600	1.14 ± 0.34	0.674 ± 0.094	10.7 ± 1.3	3.85 ± 0.23	18.4 ± 1.1	0.1514 ± 0.0090	3.94 ± 0.26
			1900	0.06 ± 0.12	0.0205 ± 0.0043	4.13 ± 0.52	2.31 ± 0.14	2.07 ± 0.12	0.1150 ± 0.0068	3.27 ± 0.21
			total	19.3 ± 1.8	16.9 ± 1.0	64.6 ± 3.0	31.34 ± 0.93	45.2 ± 1.3	1.084 ± 0.025	47.8 ± 1.2
En2I	cpx	1.029	600	1.72 ± 0.56	31.3 ± 4.1	34.5 ± 4.3	3.15 ± 0.20	2.12 ± 0.13	0.249 ± 0.015	7.17 ± 0.47
			700	2.52 ± 0.49	35.8 ± 5.0	33.8 ± 4.2	1.209 ± 0.081	0.911 ± 0.059	0.0650 ± 0.0039	2.58 ± 0.17
			800	4.71 ± 0.84	61.3 ± 8.0	57.6 ± 7.2	13.21 ± 0.79	4.35 ± 0.26	0.024 ± 0.012	6.00 ± 0.39
			1000	6.9 ± 1.7	90 ± 15	91 ± 11	3.38 ± 0.20	1.64 ± 0.10	0.1076 ± 0.0064	4.04 ± 0.26
			1200	1.54 ± 0.44	25.9 ± 3.5	122 ± 15	5.08 ± 0.30	3.69 ± 0.22	0.278 ± 0.016	11.88 ± 0.78
			1400	1.50 ± 0.45	16.1 ± 2.1	426 ± 53	12.20 ± 0.73	48.9 ± 2.9	0.497 ± 0.029	14.27 ± 0.93
			1600	0.04 ± 0.16	0.309 ± 0.048	18.4 ± 2.3	1.78 ± 0.11	3.13 ± 0.19	0.0713 ± 0.0042	2.27 ± 0.15
			total	18.9 ± 2.1	261 ± 19	784 ± 57	40.0 ± 1.2	64.7 ± 2.9	1.473 ± 0.040	48.2 ± 1.4

N.B, unit for abundance is cm^3 STP/g. All tabulated data were corrected for blanks.

Table 6
Noble gas isotopic ratios of a spinel lherzolite (stepwise heating results)

Sample	Mineral	Weight (g)	Temperatrue (°C)	$^{3}He/^{4}He$ (R/R_A)	$^{40}Ar/^{36}Ar$	$^{38}Ar/^{36}Ar$	$^{4}He/^{40}Ar^{*}$
En2I	olivine	1.512	600	1.3 ± 1.2	341.4 ± 4.0	0.1891 ± 0.0033	17.7 ± 2.8
			700	3.3 ± 1.4	369.9 ± 4.4	0.1891 ± 0.0032	15.1 ± 2.2
			800	6.5 ± 2.6	309.8 ± 3.3	0.1883 ± 0.0027	12.0 ± 1.7
			1000	22.9 ± 7.4	399.2 ± 3.0	0.1896 ± 0.0037	5.06 ± 0.78
			1200	84 ± 27	551.2 ± 5.9	0.1893 ± 0.0029	0.97 ± 0.14
			1400	220 ± 165	460.1 ± 3.5	0.1907 ± 0.0023	0.274 ± 0.046
			1600	163 ± 121	612.6 ± 5.8	0.1905 ± 0.0028	0.215 ± 0.032
			1900	45 ± 36	821.2 ± 7.0	0.1890 ± 0.0026	0.100 ± 0.020
			total	26.3 ± 1.4	484.2 ± 3.3	0.1893 ± 0.0020	1.329 ± 0.086
En2I	opx	1.575	600	2.25 ± 0.46	434.6 ± 4.7	0.1888 ± 0.0035	18.6 ± 2.7
			700	7.3 ± 2.9	348.4 ± 3.4	0.1876 ± 0.0024	4.04 ± 0.58
			800	12.6 ± 4.9	1271 ± 19	0.1891 ± 0.0052	1.50 ± 0.23
			1000	25.3 ± 8.5	986 ± 11	0.1897 ± 0.0033	1.68 ± 0.26
			1200	34 ± 11	2308 ± 27	0.1882 ± 0.0036	0.364 ± 0.052
			1400	34 ± 26	3849 ± 59	0.1909 ± 0.0046	0.067 ± 0.011
			1600	29 ± 23	4901 ± 52	0.1892 ± 0.0032	0.0380 ± 0.0058
			1900	51 ± 110	921 ± 11	0.1889 ± 0.0043	0.0142 ± 0.0031
			total	14.4 ± 1.0	1460 ± 10	0.1885 ± 0.0020	0.463 ± 0.031
En2I	cpx	1.029	600	0.45 ± 0.14	692 ± 23	0.1900 ± 0.0069	25.1 ± 3.7
			700	0.581 ± 0.090	774 ± 31	0.1900 ± 0.0093	61.9 ± 9.9
			800	0.634 ± 0.079	338.1 ± 2.3	0.1891 ± 0.0022	109 ± 16
			1000	0.63 ± 0.15	498.2 ± 6.0	0.1884 ± 0.0037	131 ± 24
			1200	0.49 ± 0.13	746.4 ± 7.1	0.1888 ± 0.0026	11.3 ± 1.7
			1400	0.80 ± 0.25	4120 ± 38	0.1918 ± 0.0027	0.346 ± 0.050
			1600	2.0 ± 8.8	1808 ± 38	0.1935 ± 0.0061	0.115 ± 0.019
			total	0.601 ± 0.059	1636 ± 12	0.1901 ± 0.0021	4.86 ± 0.38

N.B., all tabulated data were corrected for blanks. $^{40}Ar^{*}$ is ^{40}Ar corrected for air-addition.

crushing method, that is, probably in fluid inclusions. The $^{3}He/^{4}He$ ratios observed in the 1900 °C fractions of En-1, Ilc-1 and Sv-1 samples are indistinguishable from the MORB value (~ 8 R_A). Those of the other samples (Fev-1, Ba-1 and Mu-2) are also consistent with the MORB value considering their large uncertainties. A He component similar to the MORB source may therefore exist beneath Far Eastern Russia.

4.1.2. Neon

Fig. 4 presents the neon isotopic data on the three-isotope diagram. Although most samples show values that are indistinguishable from atmospheric neon within experimental uncertainties (Tables 2 and 4), some data show an excess of ^{21}Ne. There are two possibilities to explain this. One is post-eruptive cosmogenic ^{21}Ne, and the other is nucleogenic ^{21}Ne generated from (α, n) reaction on ^{18}O and (n, α) reaction on ^{24}Mg (Wetherill, 1954). Cosmogenic neon can be generated by the interaction of cosmic-ray-induced particles at the Earth's surface. Cosmogenic production ratios of $^{20}Ne/^{22}Ne$ and $^{21}Ne/^{22}Ne$ in olivine are approximately 0.84 and 0.94, respectively (Lugmair et al., 1976). Cosmogenic neon will therefore significantly affect the $^{21}Ne/^{22}Ne$ ratio due to the low abundance of ^{21}Ne in the samples. Data obtained by crushing also show a slightly high $^{21}Ne/^{22}Ne$ ratio. Since crushing minimizes contributions from nuclides in the mineral lattice (e.g. Kurz et al., 1983; Kurz, 1986; Porcelli et al., 1987; Graham et al., 1992a,b; Patterson et al., 1997; Scarsi, 2000), excess ^{21}Ne may exist in fluid inclusions as nucleogenic ^{21}Ne. However, most data obtained by crushing show values indistinguishable from atmospheric neon within experimental uncertainties. On the other hand, ratios of ^{3}He to excess ^{21}Ne calculated by correction of the atmospheric contribution are 1.7–2.7 for total gases extracted by the heating method. Such values are consistent with the reported cosmogenic production ratio of $^{3}He/^{21}Ne = 2.1$ in olivine (Marti and Craig, 1987). This means that the excess ^{21}Ne in stepwise heating data is cosmogenic in origin.

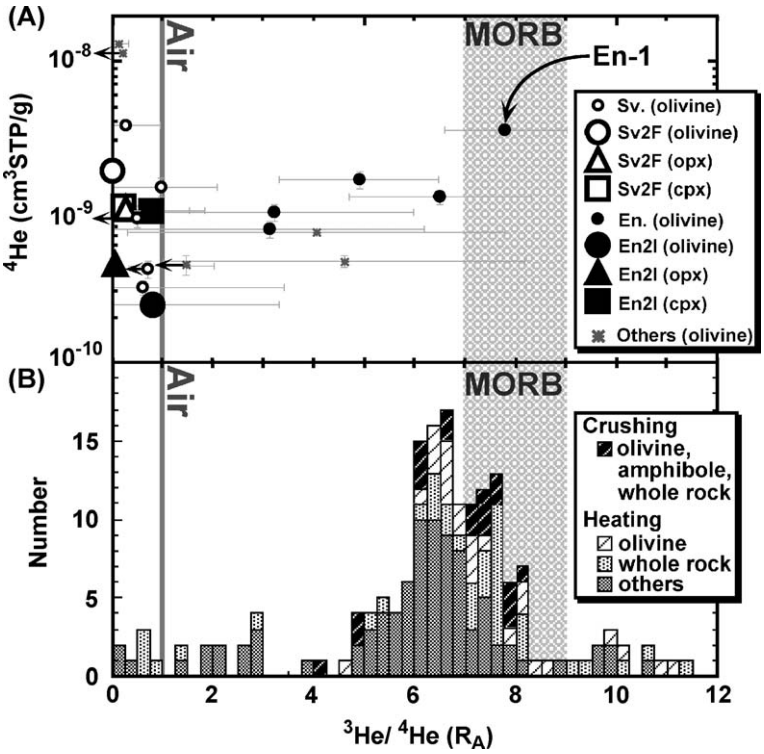

Fig. 3. (A) Helium isotope ratios of gases extracted by crushing of Ennokentiev (En.), Sveyagin (Sv.) samples. Data with uncertainties in ^{3}He/^{4}He ratio of more than 7×10^{-6} (5 R_A) are removed. (B) Histogram of ^{3}He/^{4}He ratios in continental mantle xenoliths. Data sources are as follows: north America (Dodson and Brandon, 1999; Kyser and Rison, 1982), South Africa (Kyser and Rison, 1982), Europe (Dunai and Baur, 1995; Kyser and Rison, 1982; Porcelli et al., 1986), East Africa (Porcelli et al., 1986) and south Australia (Matsumoto et al., 1997; 1998; Porcelli et al., 1986; 1992). ^{3}He/^{4}He ratios of olivine by heating are relatively higher than those of the others by heating. Quite uniform ^{3}He/^{4}He ratios are observed for samples degassed by the crushing method. Extremely low ^{3}He/^{4}He ratios are observed in gases extracted from whole rocks and other minerals by the heating method, in which low ^{3}He/^{4}He ratios are probably resulted from in-situ addition of radiogenic ^{4}He generated by decay of U and Th.

4.1.3. Argon

All ^{40}Ar/^{36}Ar ratios by crushing are less than 1000 (Table 2), significantly lower than those found in MORB (often up to 10 000 and sometimes as high as 40 000; Burnard et al., 1997). On the other hand, the heating experiments tend to yield higher ^{40}Ar/^{36}Ar ratios compared to the crushing experiments. This observation indicates accumulation of radiogenic ^{40}Ar in the crystal lattice of the samples. All the ^{38}Ar/^{36}Ar ratios are indistinguishable from the atmospheric value within the 1σ uncertainty (Tables 2, 4 and 6).

4.1.4. Krypton and xenon

Krypton and xenon isotopic ratios are indistinguishable from the atmospheric values within the experimental uncertainty at 1σ level for present samples. Although excess ^{129}Xe and excesses in heavy isotopes of xenon ($^{131-136}$Xe) relative to the atmospheric compositions have been reported for mantle-derived glasses (e.g. Staudacher and Allègre, 1982) and xenoliths (Poreda and Farley, 1992; Staudacher et al., 1990), they have not been found in the present samples.

4.2. Abundance of uranium

The concentrations of U in olivines are less than 30 ppb for all the samples analyzed in the present study (Table 3). Although occurrences of the intergranular materials and melt inclusions rich in U are possible in olivine crystals, U content of olivine in the mantle beneath Far Eastern Russia was not significantly high

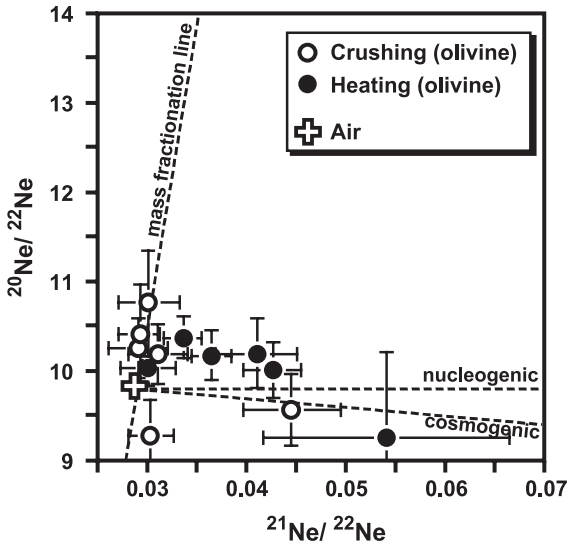

Fig. 4. Ne three-isotope diagram for the Far Eastern Russian mantle-derived xenoliths. The data obtained by the crushing and the heating methods including all temperature fractions are included. The data where the error bars overlap the air point are not plotted.

compared to those from other continents or island arcs (Wakita et al., 1967; Tolstikhin and Erlikh, 1974; Ionov et al., 1995).

5. Discussion

5.1. The occurrence of extremely low $^3He/^4He$ ratios in mantle-derived rocks

This study shows that minerals from some mantle-derived xenoliths display extremely low $^3He/^4He$ ratios for gases extracted by crushing (~ 0.3 R_A). Such low $^3He/^4He$ ratios have not been reported from olivines separated from mantle-derived xenoliths (Fig. 3). Since helium has high diffusivities in the mantle (e.g., Hart, 1984; Lux, 1987; Trull and Kurz, 1993), an extensive mantle heterogeneity would be required in order to maintain the He isotope anomaly for significant periods of time. For example, in order to maintain a source body with 6.8 R_A in a mantle with 30 R_A for 1 billion year, the thickness of the source body is required to be in the order of 1 km (Hanyu and Kaneoka, 1998). It is important to clarify the possible causes and distributions of low $^3He/^4He$ ratios.

5.1.1. Possible cause of the extremely low $^3He/^4He$ ratio in xenoliths

To explain the extremely low $^3He/^4He$ ratio observed in xenoliths, we can raise several possibilities. Below, we will discuss each of them.

5.1.1.1. Air addition. The concentration of He in the atmosphere is ~ 5 ppm and it is generally regarded to be not recycled into the mantle (e.g., Ozima and Podosek, 1983). Furthermore, the $^3He/^4He$ ratios much lower than the atmospheric value cannot be explained by mixing with the atmospheric component. Hence, air-addition cannot be the cause for low $^3He/^4He$ ratios in xenoliths.

5.1.1.2. Preferential depletion of helium. If significant He loss occurred after the formation of xenoliths, mass-dependent fractionation would lower the $^3He/^4He$ ratio significantly in minerals. To explain the observed low $^3He/^4He$ values by this process from the assumed initial MORB-like value, an anomalously high initial He concentration is required, much higher than that of popping rocks (1×10^{-4} cm^3 STP/g; Staudacher et al., 1989) which is the most gas-rich basalt glass. Since no systematic difference in noble gas concentrations in samples from different localities (Tables 1, 3 and 5) is observed, it is difficult to explain the low $^3He/^4He$ ratios by helium loss from the fluid inclusions.

5.1.1.3. Contamination by host magma and/or crustal fluids. Generally, it is thought that noble gases in fluid inclusion of mantle-derived xenolith are not affected by the host magma (e.g., Porcelli et al., 1987; Vance et al., 1989; Burnard et al., 1998). Indeed the samples En-1 and En2I, which there is no systematic difference between the samples in their depth where the samples was trapped by the host magma (Yamamoto et al., 2002), show very different helium isotopic signature. The noble gas isotopic signature for crushing experiment on natural mineral simply depends on the occurrence of inclusion.

In addition, melt inclusions are observed in all of the Far Eastern Russian mantle-derived xenoliths, but no reaction rim is observed in the boundary of the melt inclusions (Fig. A1). Further, if intense intergranular fluid flow of the host basalt occurred, it would lead to a breakup of the xenoliths, but there is no evidence for this. These observations suggest

that these xenoliths have not been pervasively contaminated by the host magma.

5.1.1.4. Accumulation of radiogenic ^{4}He after ascent of the xenoliths to the surface. In fact, there are many reports that in-situ generated helium can be released by crushing when trapped (or intrinsic) helium abundance is very low (e.g., Scarsi, 2000). In the heating experiment, however, total ^{3}He/^{4}He ratio of the En2I, which showed the lowest ^{3}He/^{4}He ratio among En-samples in the crushing experiment, was extremely high (26.3 ± 1.4 R_A; Table 6). If the gases extracted by the crushing minerals were affected by nuclides generated in situ within crystal lattice, ^{3}He/^{4}He of the En2I in the crushing experiment should be high as shown in the heating experiment. Therefore, the low ^{3}He/^{4}He ratios in crushing do not result from addition of radiogenic nuclides generated in situ after the xenoliths were transported to the surface.

5.1.1.5. Addition of radiogenic ^{4}He in the mantle. From what has been discussed above, we can conclude that the low ^{3}He/^{4}He ratio in the mantle xenoliths from Far Eastern Russia reflects an inherent feature of the Far Eastern Russian upper mantle. There are two possibilities to explain the low ^{3}He/^{4}He ratio in the mantle. One is an incorporation of mantle fluids with low ^{3}He/^{4}He ratios. The other is in-situ growth of radiogenic ^{4}He after incorporating a fluid with a high U/He ratio into the mantle material. Regarding the former possibility, some source is required to produce the mantle fluids with low ^{3}He/^{4}He ratios. For example, it is possible that the old subducted slab was stored in the upper mantle for a sufficiently long time to have accumulated enough radiogenic ^{4}He. In the latter case, for example, infiltration of U-bearing fluids into the Far Eastern Russian mantle could cause heterogeneous and low ^{3}He/^{4}He ratios. As discussed later, this latter scenario is likely because U is soluble in water at considerable depth (Brenan et al., 1995; Kogiso et al., 1997), allowing U-bearing fluids to infiltrate the mantle wedge from the subducted slab.

5.1.2. Source of the low ^{3}He/^{4}He component

The correlation between ^{4}He and ^{3}He/^{4}He ratio observed in En-series (Fig. 3) cannot result from the addition of radiogenic ^{4}He within crystal lattice after the eruption, because, as discussed before (Section 5.1.1.4), gases extracted by crushing are not affected by nuclides generated in the crystal lattice, or from melt or liquid CO_2 inclusions. Hence, the correlation seen in En-series samples must result from mixing between two components; one has a low ^{3}He/^{4}He ratio, and the other has MORB-like helium. Raman microscopic analyses indicate that the liquid CO_2 inclusions were trapped deeper than 35 km (Yamamoto et al., 2002). Since the crustal thickness has been estimated at $\sim$ 30 km for Far Eastern Russia (Karp and Leikov, 1990) and $\sim$ 34 km for the southern part of Far Eastern Russia (Zai-Yi et al., 1992), the CO_2 must be derived from the mantle. There is no systematic difference in their internal pressures between the samples En-1 and En2I. However, the concentrations of ^{4}He are significantly different between En-1 and En2I (Fig. 3). Of ten grains of olivine from En2I, only one had a trail of liquid CO_2 inclusions, while a large number of liquid CO_2 trails have been observed in all mineral separates from En-1. That is to say, the liquid CO_2 inclusions host noble gases with a ^{3}He/^{4}He ratio similar to that of MORB. However, differences in ^{3}He/^{4}He ratio cannot be explained by only the difference in liquid CO_2 inclusion density. Although noble gases are generally considered to be concentrated in CO_2-bearing inclusion trails (e.g., Farley et al., 1994; Burnard et al., 1998), melt inclusions in the present samples may have trapped noble gases. Crushing the samples of Sv-series, which contain melt inclusions, but not liquid CO_2 inclusions, yields low ^{3}He/^{4}He ratios (Fig. 5). Melt inclusions are observed in all Far Eastern Russian mantle xenoliths. Furthermore, En2I has melt inclusions similar to those of Sv-1 (Fig. 2b and c). From these observations, we infer that the low ^{3}He/^{4}He component appears to be released from the melt inclusions, while the MORB-like He is released from the liquid CO_2 inclusions. The melt inclusions are also considered to be mantle-derived fluids (see Appendix B). Initial ^{3}He/^{4}He ratios in olivine when the xenoliths were transported to the Earth's surface can be calculated by using the measured total ^{3}He/^{4}He ratio and U content in olivine and the eruption age of the host basalts. The samples Sv-1 and Fev-1, which have low ^{3}He/^{4}He ratios in the heating experiment, had initial ^{3}He/^{4}He ratios of 0.60 ± 0.08 and 0.92 ± 0.21 R_A, respectively (Fig. 6). This means that material with low ^{3}He/^{4}He ratios must have existed in the mantle xenoliths. As described in Section 4.1.1,

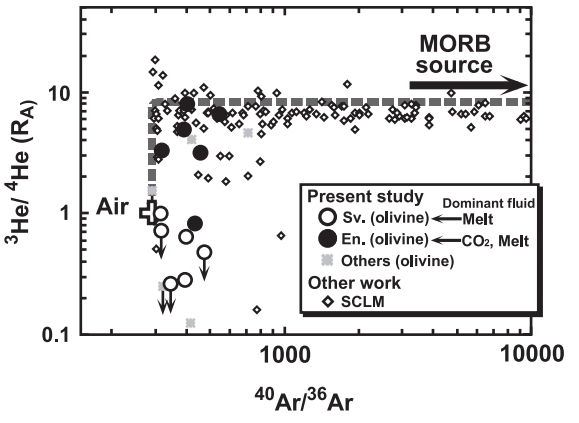

Fig. 5. The $^{3}He/^{4}He$ versus $^{40}Ar/^{36}Ar$ diagram of gases extracted by the crushing method for the Far Eastern Russian mantle-derived xenoliths in present study with data for subcontinental lithospheric mantle (SCLM). Data sources are the same as those for Fig. 3. Data with uncertainties in $^{3}He/^{4}He$ ratio of more than 7×10^{-6} (5 R_A) are removed.

the gases with low $^{3}He/^{4}He$ ratio are mostly extracted from fluid inclusions, that is, from melt inclusions. The low $^{3}He/^{4}He$ ratios might not be the result of infiltration of the melt inclusions with low $^{3}He/^{4}He$ ratios. This is because, if the melt inclusions infiltrated to the minerals as a grain boundary fluid or micro vein, the helium isotopic composition in the melt infiltration is easily homogenized with the one in the surrounding mantle during migration. Instead, these low $^{3}He/^{4}He$ ratios may result from invasion of an exotic fluid with a high U/He ratio. It seems likely that the melt inclusions, which often show a hydrous mineral on the wall of inclusion, have high U/He ratio.

The $^{4}He/^{40}Ar^{*}$ ratio can be a useful indicator for examining the fluid's source or subsequent transport processes, where $^{40}Ar^{*}$ indicates ^{40}Ar corrected for air-addition. For time scales of 10^{8} years or less, the instantaneous $^{4}He/^{40}Ar^{*}$ production ratio in the mantle is 5–20, depending on the K/U ratio assumed (13000–3000). The $^{4}He/^{40}Ar^{*}$ ratios measured in the En-series samples are relatively uniform (0.1–0.5) and significantly lower than those measured in MORB (Fig. 7), while those of samples with low $^{3}He/^{4}He$ ratios are high (~ 13.5). This seems to indicate that the liquid CO_2 fluid has $^{3}He/^{4}He$ ratios like MORB and low $^{4}He/^{40}Ar^{*}$ of ~ 0.5, and the melt inclusions have low $^{3}He/^{4}He$ ratios but relatively high $^{4}He/^{40}Ar^{*}$. Since En2I has both low $^{3}He/^{4}He$ and low $^{4}He/^{40}Ar^{*}$ ratios, the $^{3}He/^{4}He-^{4}He/^{40}Ar^{*}$ trend may indicate mixing between the two sources. A fluid with low $^{4}He/^{40}Ar^{*}$ ratio in Samoan mantle-derived xenoliths has been discussed previously by Poreda and Farley (1992) and Burnard et al. (1998). They considered that the low $^{4}He/^{40}Ar^{*}$ fluid originated in the mantle: high $^{20}Ne/^{22}Ne$ and $^{129}Xe/^{130}Xe$ ratios have been also found in xenoliths with low $^{4}He/^{40}Ar^{*}$ ratios. In addition, the low $^{4}He/^{40}Ar^{*}$ ratios were thought to have not been caused by the preferential He loss during entrainment of the xenoliths by the host magma, because inclusions with both high $^{4}He/^{40}Ar^{*}$ (up to 1.4) and low $^{4}He/^{40}Ar^{*}$ (less than 0.1) coexist in a single mineral grain (Burnard et al., 1998). The $^{4}He/^{40}Ar$ component lower than the MORB field would be a ubiquitous character of the subcontinental lithospheric mantle because such low $^{4}He/^{40}Ar$ data is fairly common in the previous study for the subcontinental lithospheric mantle (Fig. 7). Furthermore, MORB source may have a $^{4}He/^{40}Ar$ ratio lower than that of MORB. This is because, during magmatic degassing of MORB magma, the $^{4}He/^{40}Ar$ ratio of the residual volatiles will increase (e.g., Sarda and Graham, 1990) due to the

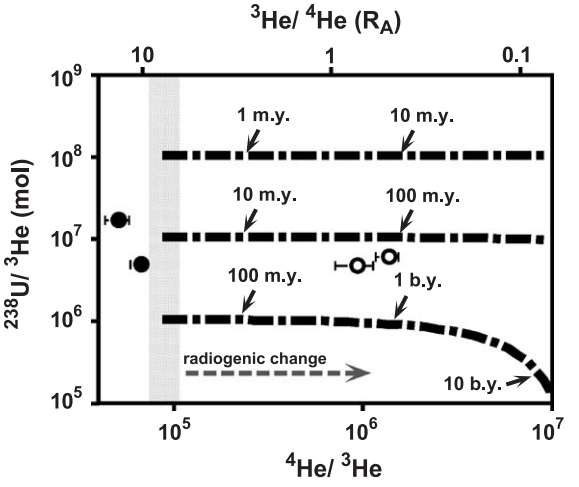

Fig. 6. $^{4}He/^{3}He$ and $^{238}U/^{3}He$ ratios in olivines. The helium isotopic contents are from data of total amount of gases extracted by heating. The thick lines show radiogenic change of the original mantle source having an initial helium isotopic ratio like MORB (shadowed area) for various $^{238}U/^{3}He$ ratios (mol) and uniform Th/U ratio of 3.1 (Staudacher et al., 1989). The thick lines are labeled with numbers that indicate time (million years (m.y.) and billion years (b.y.)).

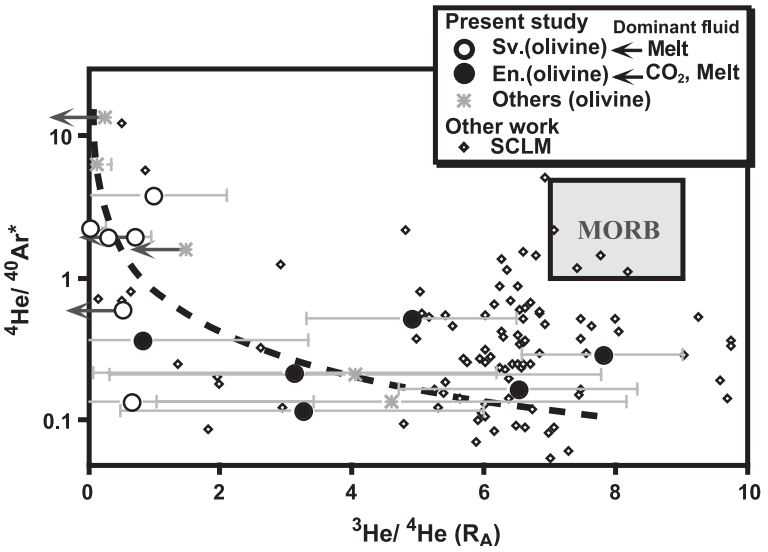

Fig. 7. $^{3}He/^{4}He$ and $^{4}He/^{40}Ar^{*}$ ratios in gases extracted by crushing method for olivine in xenoliths from localities of Ennokentiev (En.), Sveyagin (Sv.) and the others, where $^{40}Ar^{*}$ indicates ^{40}Ar corrected for air-addition. $^{4}He/^{40}Ar^{*}$ ratio of MORB is from Staudacher et al. (1989) and Moreira et al. (1998). Data sources for subcontinental lithospheric mantle (SCLM) are the same as those for Fig. 3. The broken line shows a mixing line between two original sources with $^{3}He/^{4}He$ ratio like MORB (8 R_A) and low $^{4}He/^{40}Ar$ ratio (0.1), and low $^{3}He/^{4}He$ ratio (0.1 R_A) and high $^{4}He/^{40}Ar$ ratio (15), respectively. Data with uncertainties in $^{3}He/^{4}He$ ratio of more than 7×10^{-6} (5 R_A) are removed.

greater solubility of He in silicate melts (e.g., Jambon et al., 1986).

5.2. Recycled components in the subcontinental mantle

As discussed above, the Far Eastern Russian upper mantle may have been metasomatized by an exotic melt or fluid. Such an effect should be more strongly reflected in the $^{40}Ar/^{36}Ar$ ratio, if the exotic fluid was surface-derived. $^{40}Ar/^{36}Ar$ data are low compared to MORB. The most likely source for low $^{40}Ar/^{36}Ar$ ratio gas is incorporation of atmospheric argon. The krypton and xenon isotopic ratios are indistinguishable from the atmospheric values within the experimental uncertainty at 1σ level for all data, which is consistent with the low $^{40}Ar/^{36}Ar$ ratios. Four possibilities are raised to explain the addition of the atmospheric gases into the mantle:

(1) atmospheric adsorption on the surface of the xenoliths;
(2) incorporation of surface water in xenoliths as hydrate or hydrous minerals formed by alteration after eruption of magma entraining the xenoliths;
(3) incorporation of ground water circulating within the crust into the host magma and infiltration into the xenoliths;
(4) percolation of subducted atmospheric noble gases dissolved in sea water through the mantle as the solution dehydrated from the subducted slab.

Ballentine and Barfod (2000) have argued that most atmospheric contamination might occur in the laboratory especially for heavier noble gases. However, for noble gas analysis, samples and analytical lines are always preheated in order to reduce adhered atmospheric gases. The amounts of ^{36}Ar in procedural blanks were in some cases a few orders of magnitude lower than those extracted from present samples in both crushing and heating. Furthermore, atmospheric contaminants borne by hydrous minerals generated by low temperature alteration or weathering is likely to be removed in low temperature fractions (600 °C) and by careful handpicking of mineral separates. Ballentine and Barfod (2000) have argued that the noble gas elemental compositions similar to modern air are

observed in gases extracted from the samples and that is evidence for the effect of modern air to noble gases in both MORB and OIB glasses. In the present study, however, elemental ratios of heavier noble gases measured by crushing olivine, for example $^{84}Kr/^{36}Ar$ (0.038 ± 0.020) or $^{132}Xe/^{36}Ar$ (0.0046 ± 0.0055), in which errors are expressed as 1σ for all data by crushing olivine, are not similar to the modern air value (0.021 and 0.00074, respectively). These lines of evidence suggest that possibilities (1) and (2) are not likely to explain the observed low $^{40}Ar/^{36}Ar$ ratios.

If the host magma mixed with ground water and affected the xenoliths, it would cause a decrease in the $^{40}Ar/^{36}Ar$ ratio of xenoliths. However the influence is limited to the rim of marginal minerals of the xenoliths and no reaction rim is observed at the contact between minerals and melt inclusions (Fig. A1). Melt inclusions would therefore not be directly derived from the host magma and the possibility (3) is not likely.

Low $^{40}Ar/^{36}Ar$ ratios have often been observed in samples from the subcontinental lithospheric mantle (Kyser and Rison, 1982; Dunai and Baur, 1995) and the volcanic arc mantle (Miura and Nagao, 1991; Nagao and Takahashi, 1993; Matsumoto et al., 2001). If these low $^{40}Ar/^{36}Ar$ ratios directly reflect the isotopic compositions in the mantle source, it requires that the mantle source mixed with materials with lower $^{40}Ar/^{36}Ar$ ratios, such as materials derived from subduction-related components containing atmospheric argon (Sarda et al., 1999, 2000; Matsumoto et al., 2001). In the present study, all the $^{40}Ar/^{36}Ar$ data obtained by crushing are less than 1000, and they are considered to reflect those of the fluids trapped in inclusions. Furthermore, the low $^{40}Ar/^{36}Ar$ ratios were observed irrespective of the occurrence of liquid CO_2 inclusion (Fig. 5). Accordingly, these mantle sources were probably percolated by fluid or melt derived from subduction-related components containing atmospheric argon.

5.3. Model for the evolution of the mantle wedge

Fig. 8 represents a schematic cross-section beneath the paleo-Far Eastern Russia region. In the Jurassic–early Cretaceous Period, a subduction zone was formed in Far Eastern Russia. Hydrated peridotite is formed by the addition of slab-derived H_2O beneath convergent margin with subduction zone. Hydrous minerals such as amphibole, chlorite and phlogopite in the hydrated peridotite breaks down in downward

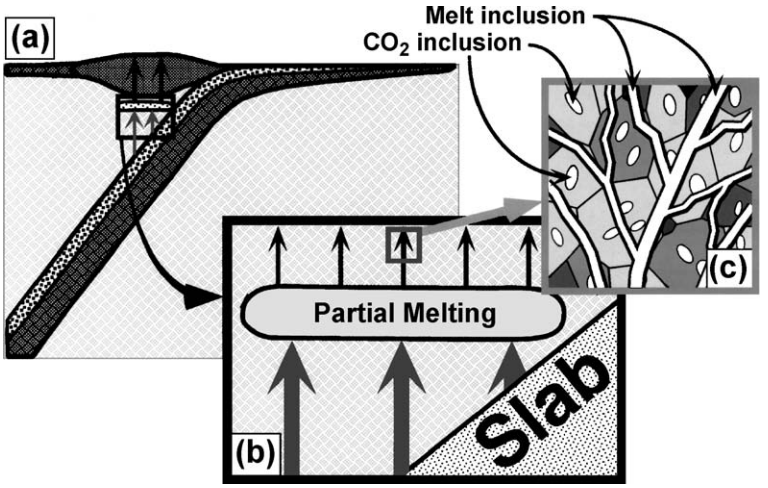

Fig. 8. (a) Schematic cross-section beneath the paleo-Far Eastern Russia. Oceanic crust subducts into the mantle wedge. (b) The figure enlarged from (a). Aqueous fluid dehydrated from subducted slab ascends into the mantle wedge. The ascending aqueous fluids trigger partial melting in the mantle wedge, which leads to generation of silicate melt. Subsequently, the silicate melt ascends through the mantle wedge. (c) A figure focused on a depth where present samples had been derived. In such a mantle, the ascending silicate melt infiltrates into the mantle and is trapped as melt inclusion. Generally, CO_2-dominant fluids ubiquitously exist in the lithospheric mantle as inclusions. Also there are liquid CO_2 inclusions in the Far Eastern Russian mantle in part.

flow of the mantle wedge and release H_2O, which ascends as fluid (e.g., Tatsumi, 1989). When the H_2O reaches the region with the solidus temperature of hydrous peridotite, partial melting in the mantle wedge takes place to produce initial magma (e.g., Kushiro, 1983; Tatsumi et al., 1983). If melt segregation occurs, melt will be extracted upwards and ascend through the mantle wedge, leading to subduction-related volcanism. Part of the melt should remain in the mantle wedge as a grain-boundary component or as melt inclusions. This melt should also contain an atmospheric component inherited from the water from the subducted slab. Also, the fluids derived from a subducted slab are likely to have inherited high U/^{3}He ratios (Farley, 1995). This is because U is mobile in water, so that it is likely to partition into aqueous fluids when the slab dehydrates (Brenan et al., 1995; Kogiso et al., 1997). The high U/^{3}He ratio in the fluids will lead to a rapid decrease in the ^{3}He/^{4}He ratio. It is noteworthy that relatively low ^{3}He/^{4}He ratios (4.2 R_A) have been reported for upper mantle-derived materials of the mantle wedge by crushing (Dodson and Brandon, 1999). Additionally, relatively low ^{40}Ar/^{36}Ar ratios have been observed in samples from the subcontinental lithospheric mantle (Kyser and Rison, 1982; Dunai and Baur, 1995) and volcanic arc samples (Miura and Nagao, 1991; Nagao and Takahashi, 1993; Matsumoto et al., 2001). This is in accordance with a model of volatile recycling via subduction supported by a large number of data on nitrogen isotopes (e.g., Bebout, 1996; Sano et al., 1998) and carbon isotopes (e.g., Sano and Marty, 1995; Nishio et al., 1998; Yamamoto et al., 2001) obtained from arc volcanic samples.

On the site of an active margin of a continent or island arc, the mantle wedge would be affected and polluted by components derived from the subducted slab shown by Matsumoto et al. (2001). However, in such areas, ^{3}He/^{4}He ratios less than the atmospheric value have not been reported. On the other hand, melt inclusions are observed in all mantle xenoliths from Far Eastern Russia, which seems to have had a low ^{3}He/^{4}He component in the mantle. In the Far Eastern Russia area, before the opening of the Japan Sea, slabs were subducted into the subcontinental mantle. If fluids derived from such subducted slab have infiltrated and remained in the mantle wedge for a sufficiently long time, they would accumulate enough radiogenic nuclides to lower the ^{3}He/^{4}He ratios to the observed values.

These processes would not be limited to the Far Eastern Russia area and relatively low ^{3}He/^{4}He and ^{40}Ar/^{36}Ar ratios have been observed in mantle materials from continental margins in previous studies (Kyser and Rison, 1982; Nagao and Takahashi, 1993; Dunai and Baur, 1995; Dodson and Brandon, 1999; Matsumoto et al., 2001) which may be attributed to the same process.

6. Conclusions

(1) Spectroscopic and petrographic observations suggest that there are at least two compositionally distinct fluids in the studied xenoliths. One is liquid inclusion filled mostly with CO_2. The other is melt inclusion often containing the bubble formed by shrinkage of the melt on cooling. Both fluids are mantle fluids.

(2) We have revealed the occurrence of extremely low ^{3}He/^{4}He ratios of less than the atmospheric value in olivine, opx and cpx for some subcontinental lithospheric mantle-derived xenoliths from Far Eastern Russia. Since He with low ^{3}He/^{4}He ratio was extracted by the crushing method, it is expected to be located mostly in fluid inclusions of minerals pervaded in the mantle. The component probably occurs in melt inclusions because low ^{3}He/^{4}He ratios are restricted to gases extracted by crushing minerals with no liquid CO_2 inclusion. On the other hand, all the samples containing liquid CO_2 inclusions tend to show relatively high ^{3}He/^{4}He ratios close to that of MORB (~8 R_A), however, with lower ^{4}He/^{40}Ar* ratio than MORB.

(3) ^{40}Ar/^{36}Ar ratios obtained by the crushing method are less than 1000. Since the low ^{40}Ar/^{36}Ar ratios are observed irrespective of the occurrence of liquid CO_2 inclusion, the atmospheric component would exist at least in melt inclusions.

(4) Far Eastern Russia was located at subduction zone in the Jurassic–Cretaceous, where fluids containing the atmospheric and radioactive isotopes derived from the subducted slab percolated into the mantle wedge. The sources of the xenoliths would therefore have been

affected by the ascending melt from the partial melting zone or the subducted slab located deeper in the mantle wedge than the sources of those xenoliths. In Far Eastern Russia, melt inclusions showing low $^{3}He/^{4}He$ and $^{40}Ar/^{36}Ar$ ratios are observed in all of the mantle xenoliths. The melt inclusions must therefore represent a component related to the subducted slab.

Acknowledgements

We thank Professors Dan N. Barfod and Harry Becker, who reviewed the manuscript and gave various useful comments on it. We appreciate Prof. K. Nagao, Prof. Y. Takigami, Dr. Y.N. Miura, Dr. N. Iwata, Dr. T. Hanyu and Dr. H. Kumagai for their help in analyzing noble gases. Prof. Y. Lai gave us suggestions on description of fluid inclusion. We thank Dr. Y. Nishio, Mr. S. Fukuda, Mr. Y. Maeda and Ms. S. Tokunaga for their help on uranium analyses. We thank Prof. T. Fujii, Prof. K. Ozawa, Prof. B. Marty, Prof. J. Matsuda, Prof. P. Sarda, Prof. H. Hiyagon, Dr. K. Mibe, Dr. H. Sumino and Ms. R. Yokochi for valuable comments and criticisms. We are much indebted to Dr. K. Sato and Ms. R. Tsurudome for permitting us to refer the unpublished results of geochronological and trace element analyses. We wish to express our deep appreciation to Drs. G.P. Glasby and P.G. Burnard for their effort to improve our English and arguments. This study has been financially supported in part by the Research Fellowships of the Japan Society for the Promotion of Science for Young Scientists to J.Y. and the Grant-in-Aid for Scientific Research by the Ministry of Education, Culture, Sports, Science and Technology in Japan to I.K. (Nos. 09440182, 09954023, 12440145).

Appendix A. Fluid inclusion and petrographic descriptions

The xenoliths from Far Eastern Russia mainly comprise spinel-lherzolites, with rare harzburgites and dunites. Garnet-lherzolite is not reported from this region. All the xenoliths used in the present study are spinel-lherzolites. Samples were collected from seven localities (Ennokentiev, Ilchanska, Sveyagin, Fevralsky, Barhatny, Muhen and Stanovoy; Fig. 1).

A.1. Ennokentiev (En-1, En-44, En-010, En-41, En2A and En2I)

Samples have allotriomorphic-granular and protogranular textures; ~1.0–2.5 mm grain size. All samples have both liquid CO_2 and melt inclusions in most constituent minerals. The liquid CO_2 inclusions usually are <10 μm in diameter and have almost negative crystal with partly spherical shape. Only one sample En-010 has coarse grain size up to 3 mm and very large liquid CO_2 inclusion of up to 50 μm in diameter in opx and cpx. Samples En-1 and En2A have a large number of liquid CO_2 trails in most mineral separates.

A.2. Ilchanska (Ilc-1 and Ilc-2)

Both samples have allotriomorphic-granular and protogranular textures. A sample Ilc-1 has coarse grain size of ~1.0–3.0 mm in diameter and does not have any liquid CO_2 inclusion. Another sample Ilc-2 is medium-grained and has liquid CO_2 inclusion like negative crystal in some constituent minerals. The size of the inclusions is <10 μm in diameter. Melt inclusions are observed in both samples.

A.3. Sveyagin (Sv-1, Sv2-10, Sv3-02, Sv-2, Sv2J, Sv2G, Sv2H and Sv2F)

Samples almost have allotriomorphic-granular and protogranular textures. They have relatively coarse grain size of ~1.0–3.0 mm in diameter. A sample Sv-1 has protogranular to porphyroclastic texture and grain size of 0.2–2.0 mm. Although liquid CO_2 inclusions are rarely observed in olivines of samples Sv-1 and Sv2H, all the other samples do not have liquid CO_2 inclusion at all. The size of the liquid CO_2 inclusions in samples Sv-1 and Sv2H is <5 μm in diameter. Melt inclusions are observed in all samples.

A.4. Fevralsky (Fev-1, Fev#-4 and Fev-16)

Samples Fev-1 and Fev#-4 have allotriomorphic-granular and protogranular textures. The grain

size is relatively coarse ranging from ~1.0 to 3.0 mm in diameter. A sample Fev-16 has allotriomorphic-granular and porphyroblastic textures. The grain size ranges from 1.5 to 3.0 mm in diameter. Liquid CO_2 inclusions are not observed in any samples. Melt inclusions are observed in all samples.

A.5. Barhatny (Ba-1, Ba-2, Ba-17 and Ba-18)

Samples almost have allotriomorphic-granular and protogranular textures. A sample Ba-1 has allotriomorphic-granular and porphyroblastic textures. The grain size is relatively fine ranging from ~1.0 to 2.0 mm in diameter. Liquid CO_2 inclusions are observed in opx and cpx of sample Bch-18. The liquid CO_2 inclusions are <10 μm in diameter and have almost negative crystal with partly spherical shape. Melt inclusions are observed in all samples.

A.6. Muhen (Mu-2)

Sample has allotriomorphic-granular and protogranular textures; ~2.0–2.5 mm grain size. It has only melt inclusions.

A.7. Stanovoy (St-5)

Sample has allotriomorphic-granular and protogranular textures; ~1.5–2.0 mm grain size. Liquid CO_2 inclusions are observed in an olivine. The liquid CO_2 inclusions are <5 μm in diameter and have negative

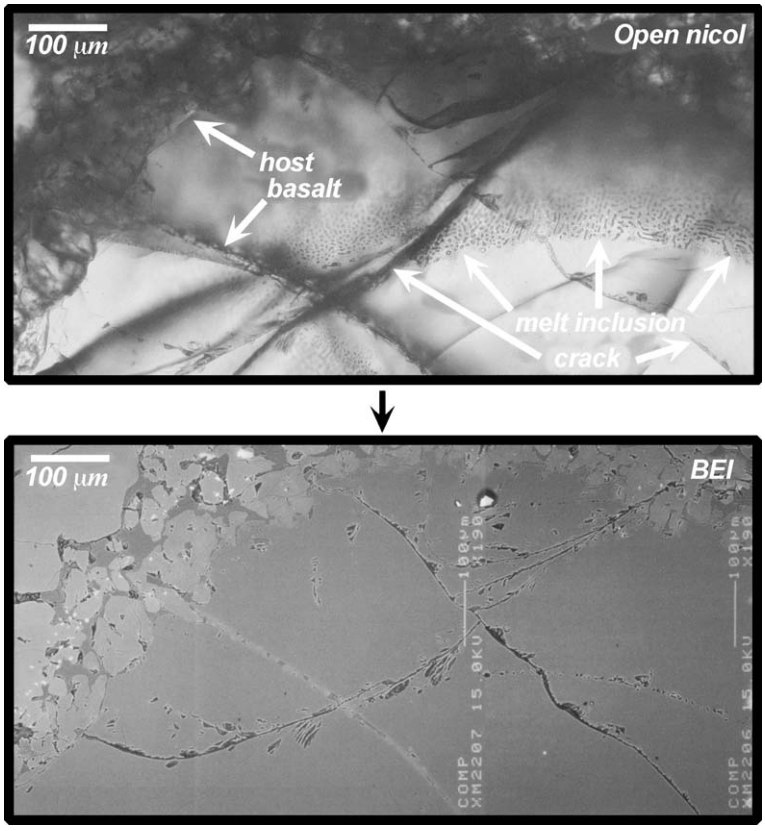

Fig. A1. Photomicrographs of a thick section of mantle-derived xenolith (Ilc-1) from the Far Eastern Russia, which are photographs of the grain boundary between olivine and orthopyroxene. Upper photo was taken under an open nicol. Lower one is BEI. Both the intergranular host magma and melt inclusion are shown. Although the host magma infrequently intrude into the mineral and show a reacted part as observed in marginal minerals of xenoliths, such a reaction is not observed in a part where melt inclusions emerge.

crystal with partly spherical shape. Melt inclusions are observed in all minerals.

Appendix B. Relationship between host magma, inclusions of liquid CO_2 and melt

The liquid CO_2 inclusions would have been trapped by minerals in the mantle because the arrays of the liquid CO_2 inclusions do not crosscut grain boundaries. In contrast, the melt inclusions are aligned along with healed fractures and frequently crosscut grain boundaries (Fig. 2a). Further, the liquid CO_2 inclusions associated with the melt inclusions often contain vapor bubbles. The data from cryogenic microthermometry indicate that the liquid CO_2 inclusions showing low density obviously decrepitated or were penetrated by the melt inclusions (Yamamoto et al., 2002). Such low density of the CO_2 could be attributed to partial loss of CO_2 from the inclusion by decrepitation or intrusion of the melt. Hence the melt intruded minerals after incorporation of the CO_2. As observed in Fig. 2a, the distribution of the melt inclusions through the grain boundary was well preserved in the xenoliths. This indicates that the mantle rock has not rheologically flowed after the intrusion of the melt.

Generally, when xenoliths have suffered heating episodes caused by the host magma, they show reaction coronae surrounding the xenoliths. However, such a rim is not observed at the contact with melt inclusions (Fig. A1). Since the Far Eastern Russian mantle xenoliths are inferred to have ascended to the Earth's surface within ten days (Yamamoto et al., 2002), chance for intrusion of the host magma into the xenolith may be limited during the period. If the melt inclusions were derived from the host magma, it is impossible to explain the observation that the rim is not observed around the melt inclusions, but exists around micro veins of the host magma as observed in Fig. A1. This is because it takes more than a few years to wipe out the rim completely (for example, it takes about five hundred days for Mg to diffuse for 10 μm at 1000 °C; Sockel and Hallwig, 1977). Therefore the melt present in melt inclusions would not be directly related to the host magma, but would be a fluid percolating into the Far Eastern Russian mantle prior to the entrainment of xenoliths by the host magma.

References

Arai, S., 1987. An estimation of the least depleted spinel peridotite on the basis of olivine-spinel mantle array. Neues Jahrb. Mineral., Monatsh. 8, 347–354.

Ballentine, C.J., Barfod, D.N., 2000. The origin of air-like noble gases in MORB and OIB. Earth Planet. Sci. Lett. 180, 39–48.

Bebout, G.E., 1996. Volatile transfer and recycling at convergent margins: mass-balance and insights from high-P/T metamorphic rocks. In: Bebout, G.E., Scholl, D.W., Kirby, S.H., Platt, J.P. (Eds.), (Eds.), Subduction: Top to Bottom. AGU Geophys. Monogr., vol. 96, pp. 179–193.

Brenan, J.M., Shaw, H.F., Ryerson, F.J., Phinney, D.L., 1995. Mineral-aqueous fluid partitioning of trace elements at 900C and 2.0 GPa: constraints on the trace element chemistry of mantle and deep crust fluids. Geochim. Cosmochim. Acta 59, 3331–3350.

Burnard, P.G., Graham, D., Turner, G., 1997. Vesicle-specific noble gas analyses of "popping rock": implications for primordial noble gases in earth. Science 276, 568–571.

Burnard, P.G., Farley, K.A., Turner, G., 1998. Multiple fluid pulses in a Samoan harzburgite. Chem. Geol. 147, 99–114.

Burrett, C.F., 1974. Plate tectonics and the fusion of Asia. Earth Planet. Sci. Lett. 21, 181–189.

Craig, H., Lupton, J.E., 1976. Primordial neon, helium, and hydrogen in oceanic basalts. Earth Planet. Sci. Lett. 31, 369–385.

Dodson, A., Brandon, A.D., 1999. Radiogenic helium in xenoliths from Simcoe, Washington, USA: implications for metasomatic processes in the mantle wedge above subduction zones. Chem. Geol. 160, 371–385.

Dunai, T.J., Baur, H., 1995. Helium, neon, and argon systematics of the European subcontinental mantle: implications for its geochemical evolution. Geochim. Cosmochim. Acta 59, 2767–2783.

Farley, K.A., 1995. Rapid cycling of subducted sediments into the Samoan mantle plume. Geology 23, 531–534.

Farley, K.A., Poreda, R.J., Onstott, T.C., 1994. Noble gases in deformed xenoliths from an ocean island: characterization of a metasomatic fluid. In: Matsuda, J. (Ed.), (Ed.), Noble Gas Geochemistry and Cosmochemistry. Terra Scientific Publishing, Tokyo, Japan, pp. 159–178.

Faure, M., Natal'in, B.A., 1992. The geodynamic evolution of the eastern Eurasian margin in Mesozoic times. Tectonophysics 208, 397–411.

Gautheron, C., Moreira, M., 2002. Helium signature of the subcontinental lithospheric mantle. Earth Planet. Sci. Lett. 199, 39–47.

Graham, D.W., Humphris, S.E., Jenkins, W.J., Kurz, M.D., 1992a. Helium isotope geochemistry of some volcanic rocks from Saint Helena. Earth Planet. Sci. Lett. 110, 121–131.

Graham, D.W., Jenkins, W.J., Schilling, J.-G., Thompson, G., Kurz, M.D., Humphris, S.E., 1992b. Helium isotope geochemistry of mid-ocean ridge basalts from the South Atlantic. Earth Planet. Sci. Lett. 110, 133–147.

Hanyu, T., Kaneoka, I., 1998. Open system behavior of helium in case of the HIMU source area. Geophys. Res. Lett. 25, 687–690.

Hanyu, T., Kaneoka, I., Nagao, K., 1999. Noble gas study of HIMU and EM ocean island basalts in the Polynesian region. Geochim. Cosmochim. Acta 63, 1181–1201.

Hart, S.R., 1984. He diffusion in olivine. Earth Planet. Sci. Lett. 70, 297–302.

Ionov, D.A., Prikhod'ko, V.S., O'Reilly, S.Y., 1995. Peridotite xenoliths in alkali basalts from the Sikhote-Alin, southeastern Siberia, Russia: trace-element signatures of mantle beneath a convergent continental margin. Chem. Geol. 120, 275–294.

Jambon, A., Weber, H.W., Braun, O., 1986. Solubility of He, Ne, Ar, Kr, and Xe in a basalt melt in the range 1250–1600 °C. Geochemical implications. Geochim. Cosmochim. Acta 50, 401–408.

Kaneoka, I., 1983. Noble gas constraints on the layered structure of the mantle. Nature 302, 698–700.

Karp, B., Leikov, E.P., 1990. Geological structure, composition and evolution of crustal layers of the Japan Sea. Tectonophysics 181, 277–283.

Kogiso, T., Tatsumi, Y., Nakano, S., 1997. Trace element transport during dehydration processes in the subducted oceanic crust: 1. Experiments and implications for the origin of ocean island basalts. Earth Planet. Sci. Lett. 148, 193–205.

Kurz, M.D., 1986. Cosmogenic helium in a terrestrial igneous rock. Nature 320, 435–439.

Kurz, M., Jenkins, W.J., 1981. The distribution of helium oceanic basaltic glasses. Earth Planet. Sci. Lett. 53, 41–54.

Kurz, M.D., Jenkins, W.J., Hart, S.R., Clague, D., 1983. Helium isotopic variations in volcanic rocks from Loihi Seamount and the Island of Hawaii. Earth Planet. Sci. Lett. 66, 388–406.

Kushiro, I., 1983. On the lateral variation in chemical composition and volume of Quaternary volcanic rocks across Japanese arcs. J. Volcanol. Geotherm. Res. 18, 435–447.

Kyser, T.K., Rison, W., 1982. Systematics of rare gas isotopes in basic lavas and ultramafic xenoliths. J. Geophys. Res. 87, 5611–5630.

Lugmair, G.W., Marti, K., Kurtz, J.P., Scheinin, N.B., 1976. History and genesis of lunar troctolite 76535 or: how old is old? Proc. Lunar. Sci. Conf. VII, 2009–2033.

Lux, G., 1987. The behaviour of noble gases in silicate liquids: solution, diffusion, bubbles and surface effects, with applications to natural samples. Geochim. Cosmochim. Acta 51, 1549–1560.

Marti, K., Craig, H., 1987. Cosmic ray produced neon and helium in the summit lavas of Maui. Nature 325, 335–337.

Maruyama, S., Sakai, H., 1986. Tectonics of Asia as a composite continent. Monogr. Assoc. Geol Collab. Japan 31, 487–518.

Matsuda, J., Matsumoto, T., Sumino, H., Nagao, K., Yamamoto, J., Miura, Y., Kaneoka, I., Takahata, N., Sano, Y., 2002. The $^{3}He/^{4}He$ ratio of the new internal He standard of Japan (HESJ). Geochem. J. 36, 191–195.

Matsumoto, T., Honda, M., McDougall, I., Yatsevich, I., O'Reilly, S.Y., 1997. Plume-like neon in a metasomatic apatite from the Australian lithospheric mantle. Nature 388, 162–164.

Matsumoto, T., Honda, M., McDougall, I., O'Reilly, S.Y., 1998. Noble gases in anhydrous lherzolites from the Newer Volcanics, southeastern Australia: a MORB-like reservoir in the subcontinental mantle. Geochim. Cosmochim. Acta 62, 2521–2533.

Matsumoto, T., Honda, M., McDougall, I., O'Reilly, S.Y., Norman, M., Yaxley, G., 2000. Noble gases in pyroxenites and metasomatised peridotites from the Newer Volcanics, southeastern Australia: implications for mantle metasomatism. Chem. Geol. 168, 49–73.

Matsumoto, T., Chen, Y., Matsuda, J., 2001. Concomitant occurrence of primordial and recycled noble gases in the Earth's mantle. Earth Planet. Sci. Lett. 185, 35–47.

Miura, Y., Nagao, K., 1991. Noble gases in six GSJ igneous rock samples. Geochem. J. 25, 163–171.

Moore, J.G., 1979. Vesicularity and CO_2 in mid-ocean ridge basalt. Nature 282, 250–253.

Moreira, M., Kunz, J., Allègre, C.J., 1998. Rare gas systematics in popping rock: isotopic and elemental compositions in the upper mantle. Science 279, 1178–1181.

Nagao, K., Takahashi, E., 1993. Noble gases in the mantle wedge and lower crust: an inference from the isotopic analyses of xenoliths from Oki-Dogo and Ichinomegata, Japan. Geochem. J. 27, 229–240.

Nishio, Y., Sasaki, S., Gamo, T., Hiyagon, H., Sano, Y., 1998. Carbon and helium isotope systematics of North Fiji Basin basalt glasses: carbon geochemical cycle in the subduction zone. Earth Planet. Sci. Lett. 154, 127–138.

Okamura, S., Martynov, Y.A., Furuyama, K., Nagao, K., 1998. K–Ar ages of the basaltic rocks from Far East Russia: Constraints on the tectono-magmatism associated with the Japan Sea opening. Isl. Arc 7, 271–282.

Ozima, M., Podosek, F.A., 1983. Noble Gas Geochemistry. Cambridge Univ. Press, Cambridge.

Patterson, D.B., Farley, K.A., McInnes, B.I.A., 1997. Helium isotopic composition of the Tabar-Lihir-Tanga-Feni island arc, Papua New Guinea. Geochim. Cosmochim. Acta 61, 2485–2496.

Porcelli, D., O'Nions, R.K., O'Reilly, S.Y., 1986. Helium and strontium isotopes in ultramafic xenoliths. Chem. Geol. 54, 237–249.

Porcelli, D.R., Stone, J.O.H., O'Nions, R.K., 1987. Enhanced $^{3}He/^{4}He$ ratios and cosmogenic helium in ultramafic xenoliths. Chem. Geol. 64, 25–33.

Porcelli, D.R., O'Nions, R.K., Galer, S.J.G., Cohen, A.S., Mattey, D.P., 1992. Isotopic relationships of volatile and lithophile trace elements in continental ultramafic xenoliths. Contrib. Mineral. Petrol. 110, 528–538.

Poreda, R.J., Farley, K.A., 1992. Rare gases in Samoan xenoliths. Earth Planet. Sci. Lett. 113, 129–144.

Rasskazov, S.V., Boven, A., Ivanov, A.V., Semenova, V.G., 2000. Middle quaternary volcanic impulse in the Olekma-Stanovoy mobile system: $^{40}Ar-^{39}Ar$ dating of volcanics from the Tokinsky Stanovik. Tikhookeanskaya Geol. Mag. 19, 19–28.

Rison, W., 1980. Isotopic studies of the rare gases in igneous rocks: implications for the mantle and atmosphere. PhD thesis. University of California. Berkeley.

Sano, Y., Marty, B., 1995. Origin of carbon in fumarolic gas from island arcs. Chem. Geol. 119, 265–274.

Sano, Y., Takahata, N., Nishio, Y., Marty, B., 1998. Nitrogen recycling in subduction zones. Geophys. Res. Lett. 25, 2289–2292.

Sarda, P., Graham, D., 1990. Mid-ocean ridge popping rocks: implications for degassing at ridge crests. Earth Planet. Sci. Lett. 97, 268–289.

Sarda, P., Moreira, M., Staudacher, T., 1999. Argon-lead isotopic correlation in Mid-atlantic ridge basalts. Science 283, 666–668.

Sarda, P., Moreira, M., Staudacher, T., Schilling, J.-G., Allègre, C.J., 2000. Rare gas systematics on the southernmost Mid-Atlantic Ridge: constraints on the lower mantle and the Dupal source. J. Geophys. Res. 105, 5973–5996.

Sato, K., 1999. Cenozoic volcanism in northern Sikhote Alin, Far East Russia and its implication for the opening of the Japan Sea. PhD thesis. University of Kyoto.

Scarsi, P., 2000. Fractional extraction of helium by crushing of olivine and clinopyroxene phenocrysts: effects on the $^{3}He/^{4}He$ measured ratio. Geochim. Cosmochim. Acta 64, 3751–3762.

Sockel, H.G., Hallwig, D., 1977. Ermittlung kleiner diffusions koeffizienten mittels SIMS in oxydischen verbindungen. Mikrochim. Acta 7, 95–107.

Staudacher, T., Allègre, C.J., 1982. Terrestrial xenology. Earth Planet. Sci. Lett. 60, 389–406.

Staudacher, T., Sarda, P., Richardson, S.H., Allègre, C.J., Sagna, I., Dimitriev, L.V., 1989. Noble gases in basalt glasses from a Mid-Atlantic Ridge topographic high at 14′ N: geodynamic consequences. Earth Planet. Sci. Lett. 96, 119–133.

Staudacher, T., Sarda, P., Allègre, C.J., 1990. Noble gas systematics of Réunion Island, Indian Ocean. Chem. Geol. 89, 1–17.

Sumino, H., Nagao, K., Notsu, K., 2001. Highly sensitive and precise measurement of helium isotopes using a mass spectrometer with double collector system. J. Mass Spectrom. Soc. Jpn. 49, 61–68.

Tatsumi, Y., 1989. Migration of fluid phases and genesis of basalt magmas in subduction zones. J. Geophys. Res. 94, 4697–4707.

Tatsumi, Y., Sakuyama, M., Fukuyama, H., Kushiro, I., 1983. Generation of arc basalt magmas and thermal structure of the mantle wedge in subduction zones. J. Geophys. Res. 88, 5815–5825.

Tatsumi, Y., Sato, K., Sano, T., Arai, R., Prikhodko, V.S., 2000. Transition from arc to intraplate magmatism associated with backarc rifting: evolution of the Sikhote Alin volcanism. Geophys. Res. Lett. 27, 1587–1590.

Tolstikhin, I.N., Erlikh, E.N., 1974. Isotopic composition of helium in ultrabasic xenoliths from volcanic rocks of Kamchatka. Earth Planet. Sci. Lett. 22, 75–84.

Trull, T.W., Kurz, M.D., 1993. Experimental measurements of ^{3}He and ^{4}He mobility in olivine and clinopyroxene at magmatic temperatures. Geochim. Cosmochim. Acta 57, 1313–1324.

Trull, T.W., Kurz, M.D., Jenkins, W.J., 1991. Diffusion of cosmogenic ^{3}He in olivine and quartz: implications for surface exposure dating. Earth Planet. Sci. Lett. 103, 241–256.

Vance, D., Stone, J.O.H., O'Nions, R.K., 1989. He, Sr and Nd isotopes in xenoliths from Hawaii and other oceanic islands. Earth Planet. Sci. Lett. 96, 147–160.

Wakita, H., Nagasawa, H., Uyeda, S., Kuno, H., 1967. Uranium, thorium and potassium contents of possible mantle materials. Geochem. J. 1, 183–198.

Wetherill, G.W., 1954. Variations in the isotopic abundances of neon and argon extracted from radioactive minerals. Phys. Rev. 96, 679–683.

Yamamoto, J., 2001. Investigation of the subcontinental mantle based on noble gas isotopes, petrological and spectroscopic studies of Siberian mantle xenoliths. PhD thesis. University of Tokyo. 132 pp.

Yamamoto, J., Watanabe, M., Nozaki, Y., Sano, Y., 2001. Helium and carbon isotopes in fluorites: implications for mantle carbon contribution in an ancient subduction zone. J. Volcanol. Geotherm. Res. 107, 19–26.

Yamamoto, J., Kagi, H., Kaneoka, I., Lai, Y., Prikhod'ko, V.S., Arai, S., 2002. Fossil pressures of fluid inclusions in mantle xenoliths exhibiting rheology of mantle minerals. Earth Planet. Sci. Lett. 198, 511–519.

Zai-Yi, T., Ping, H., Ke-Ding, X., 1992. The mesozoic–cenozoic east China rift system. Tectonophysics 208, 341–363.